

1-1-2009

A mobile mapping system utilizing a spherical camera

Craig Alleva
Ryerson University

Follow this and additional works at: <http://digitalcommons.ryerson.ca/dissertations>

 Part of the [Geographic Information Sciences Commons](#)

Recommended Citation

Alleva, Craig, "A mobile mapping system utilizing a spherical camera" (2009). *Theses and dissertations*. Paper 504.

This Thesis is brought to you for free and open access by Digital Commons @ Ryerson. It has been accepted for inclusion in Theses and dissertations by an authorized administrator of Digital Commons @ Ryerson. For more information, please contact bcameron@ryerson.ca.

619580836

GA
139
ACK
0009

A MOBILE MAPPING SYSTEM UTILIZING A SPHERICAL CAMERA

By

Craig Alleva

B.A.Sc Geomatics Engineering, York

Toronto, Ontario, Canada, 2006

A thesis presented to Ryerson University
in partial fulfillment of the requirements for the
degree of Masters of Applied Science
in the program of Civil Engineering

Toronto, Ontario, Canada, 2009

© Craig Alleva, 2009

PROPERTY OF
RYERSON UNIVERSITY LIBRARY

Author's Declaration

I hereby declare that I am the sole author of this thesis.

I hereby provide Ryerson University to lend this thesis to other educational institutions for purposes of scholarly research only.

Furthermore, I authorize Ryerson University to reproduce this thesis by photocopying or by other means, in total or in part, at the request of other educational institutions or individuals for the purposes of scholarly research

Abstract

A MOBILE MAPPING SYSTEM UTILIZING A SPHERICAL CAMERA

Craig Alleva

M.A.Sc, Civil Engineering, Ryerson University, 2009

The transportation departments belonging to respective provinces currently collect highway management data with the use of several methods and systems which include visual field inspections, survey methods, aerial photogrammetry, as well as mobile data acquisition systems. Spherical cameras offer an attractive alternative to standard mobile data acquisition devices for highway management systems as they provide full coverage with a single camera. Inclusion of such a camera requires methods of determining relative, interior and exterior orientation information, as well as bore-sight and lever arm determination. Specialized methods of mosaicking the imagery are also required. This paper focuses on exploring these methods for spherical cameras. Several computer programs were developed to solve for relative, interior, and exterior orientation parameters. It was concluded that a spherical camera can be efficiently utilized for highway data collection and provides full data coverage with a single camera system.

Acknowledgements

I would like to first thank Dr. Michael Chapman, who has provided me with tremendous support throughout my thesis, and has offered his expertise, knowledge, patience, and kindness, all of which has assisted me in the completion of this thesis. Without his guidance and help, this thesis may not have been completed. I could not ask for a better supervisor.

I would also like to extend my deepest gratitude for my fellow colleagues at PCI Geomatics, whom offered me further guidance and assistance during the writing of this thesis. Most notably, I would like to thank James Lutes for his continued advice and his willingness to assist and answer questions whenever I needed extra help. His expertise and experience was truly a blessing.

My sincere thanks also goes out to Yubin Xin, of PCI Geomatics, for his advice and guidance in the field of Mobile Mapping, and for allowing me to bounce ideas off him.

The Department of Graduate Studies, Civil Engineering, and specifically Mary Neelands, for her countless efforts to assist me in all my administrative issues.

Finally, I would like to thank my parents for their continued support throughout my university career, and for believing in me, and always being there when times were difficult.

Table of Contents

AUTHORS DECLARATION	ii
ABSTRACT	iii
ACKNOWLEDGEMENTS	iv
LIST OF TABLES	vi
LIST OF FIGURES	vii
LIST OF APPENDICES	viii
CHAPTER 1 INTRODUCTION	1
1.1 Mobile Mapping.....	1
1.2 Principles of Mobile Mapping.....	2
1.2.1 Sensors.....	2
1.2.2 Positioning.....	3
1.2.3 Orientation.....	4
1.2.4 Full System Integration.....	5
1.3 Research Objectives.....	7
CHAPTER 2 COLLINEARITY EQUATIONS	9
CHAPTER 3 CAMERA CALIBRATION	11
3.1 Immersive Media Dodecahedron Camera.....	11
3.2 Interior Orientation Parameters.....	13
3.2.1 Principal Point Coordinate and Scale Factor Determination.....	13
3.2.2 Lens Distortion Parameters Determination.....	14
3.3 Relative Orientation Determination.....	15
CHAPTER 4 SOLVING FOR INTERIOR ORIENTATION PARAMETERS	27
CHAPTER 5 DIRECT AND INDIRECT GEOREFERENCING	35
5.1 Indirect Georeferencing.....	35
5.2 Direct Georeferencing.....	36
CHAPTER 6 BORE-SIGHT AND LEVER ARM DETERMINATION	37
6.1 Bore-sight Angle Determination.....	40
6.2 Lever Arm Determination.....	41
CHAPTER 7 IMAGE MOSAICKING WITH A SPHERICAL CAMERA	43
7.1 Geometric Correction for Image Mosaicking.....	44
7.2 Color Balancing and Seam Line Elimination.....	48
7.2.1 Color Balancing (Histogram Matching).....	49
7.2.2 Seam Line Definition.....	50
7.2.3 Seam Smoothing.....	50
7.3 Potential Problems with Approach.....	51
CHAPTER 8 CONCLUSIONS AND FUTURE WORK TO BE DONE	53
REFERENCES	56

List of Tables

Table 3.1 – List of Cameras and their Associated Position and Orientation Information.....	25
Table 4.1 – List of Cameras and their Associated Position and Orientation for Virtual Point Production.....	29
Table 4.2 – List of Cameras and their Associated Interior Orientation Information for Virtual Point Production.....	29
Table 4.3 – List of Cameras and their Associated Position and Orientation as Determined By Self-Calibrating Bundle Adjustment.....	33
Table 4.4 – List of Cameras and their Associated Interior Orientation Information as Determined by Self-Calibrating Bundle Adjustment.....	34

List of Figures

Figure 1.1: Angular Orientation Parameters.....	4
Figure 1.2: Detailed Diagram of Elements of Georeferencing for Close-Range Case.....	6
Figure 2.1: Principle of Collinearity Equations.....	9
Figure 3.1: Dodecahedron.....	11
Figure 3.2: Dodeca 2360.....	12
Figure 3.3: Regular Pentagon – Side Length 1.....	15
Figure 3.4: Regular Pentagon with Local 2D Coordinate Frame Superimpose.....	16
Figure 3.5: Mathematical Relationships of a Regular Pentagon.....	17
Figure 3.6: Vertices of a Regular Pentagon.....	18
Figure 3.7: Pentagon with V4 Centered on Origin, followed by Rotation of 64 Degrees about X-Axis, followed by Rotation of 108 Degrees about the Z-Axis.....	19
Figure 3.8: Upper Right Face of Dodecahedron with Reference Top Face.....	20
Figure 3.9: Complete 2D Representation of Upper Portion of Dodecahedron.....	21
Figure 3.10: Completed 2D Representation of Lower Portion of Dodecahedron.....	21
Figure 3.11: Compute Vectors V3V1, V4V1, Bi-Sector.....	23
Figure 3.12: Front View of Dodecahedron.....	26
Figure 3.13: Top View of Dodecahedron.....	26
Figure 4.1: Virtual Sphere of Points Centered at Centre of Dodecahedron.....	28
Figure 4.2: Example Image Coordinate System Utilized.....	30
Figure 6.1: Detailed Diagram of Elements of Georeferencing for Close-Range Case.....	38
Figure 7.1: Projecting Image onto Surface of the Sphere.....	44
Figure 7.2: Mosaic Generated by Immersive Media using Data Captured by Dodeca 2360...	46
Figure 7.3: Super-Imposed Spherical Coordinate System on Mosaic.....	46
Figure 7.4: Image Edge Points Plotted onto Immersive Media Mosaic Grid.....	47
Figure 7.5: Minimum Bounding Box Encompassing Image on Mosaic.....	47

List of Appendices

APPENDIX A – NORMAL EQUATIONS STRUCTURE.....	54
--	----

1. Introduction

1.1 Mobile Mapping

In the past decade, expansion and growth of urban areas has occurred rapidly. The occurrence of rapid growth requires city planners to have access to detailed and recent information related to location and control for sites under development. The high demand for location information can also most recently be seen in Alberta, where development has been booming over the last few years. With the rising demand of location information, Geographic Information Systems which are spatially referenced have been developed. The information contained within a Geographic Information System have been collected via various methods, such as surveying and GPS point collection, however these methods are often expensive and provide only point information, rather than full coverage. An additional drawback of these methods is that they are often time consuming, and do not answer, “increasingly complex questions concerning the interaction of different factors in urban centers and their time dependencies.” (El-Sheimy, pg 1, 1996). Fortunately, the field of photogrammetry (both aerial and close-range types) has developed and can provide a solution to rapid data collection which conventional methods fail to realize. One such solution is the deployment of a mobile mapping system.

Mobile mapping has been around for decades, but until recently has not gained as much attention as it now does today. This was due primarily to the fact that Mobile Mapping Systems (MMS) were, in the past, heavily restricted to areas of application in which the exterior orientation parameters of the cameras/sensors onboard the vehicle could be easily determined. This meant that mobile mapping activities had to be conducted in such a way so that the exterior orientation parameters could be derived from ground control points. However, over the last decade, significant advances in satellite technology, as well as inertial navigation technology, have removed this restriction from MMS's. Mobile Mapping Systems can now operate virtually anywhere, and thus the need for ground control points has vanished. Further advances in technology have resulted in a transition from the traditional analog based methods of image collection (i.e., film) to digital based methods of image collection. These advances have now resulted in a mobile mapping system which contain various sensors and image capturing devices, as well as the capability to acquire, store and process georeferenced data.(Schwarz et. al 2004).

1.2 Principles of Mobile Mapping

Mobile mapping systems operate primarily on photogrammetric principles and, like traditional photogrammetric platforms, include some type of sensor used to image the area of interest, as well as a positioning device, and an orientation device. Each of these components will be discussed herein.

1.2.1 Sensors

In the field of photogrammetry, the most important device is the sensor for which the system uses to image the area of interest. Two different types of sensors exist; active sensors and passive sensors. An active sensor is a sensor which provides its' own source of energy to illuminate the area of interest. The sensor operates by emitting energy, in the form of electromagnetic energy, which interacts with the target (area of interest) and is then reflected back to the sensor where it is detected, measured and then recorded by the sensor system. The most prominent advantage of these types of sensors is that they can be operated at any time of day.

A passive sensor is a sensor which uses the sun as its source of energy. When electromagnetic radiation (from the sun for example) interacts with the target (area of interest), it is reflected or emitted and is detected, measured and recorded by the passive sensor. These sensors do not have their own source of radiant energy.

In photogrammetry, the sensor most commonly employed is the camera. A standard camera works by recording, "the image of an exterior object [which] is projected upon a sensitized plate or film, through an opening usually equipped with a lens or lenses, shutter, and variable aperture." (Wolf et al, 2000). Recently, the advent of digital cameras has resulted in these devices finding their way into photogrammetry. The digital camera operates by detecting electromagnetic energy with the use of some type of solid-state detector. The most common type of solid-state detector currently in use is known as the charged-coupled device (CCD). These devices operate by detecting electromagnetic radiation which is incident upon one of the CCD elements at a pixel location. The CCD element then generates an electrical charge which is in proportion to the intensity of the electromagnetic radiation which was incident upon the CCD element. "The electric charge is subsequently amplified and converted from analog to digital form." (Wolf et al, 2000).

1.2.2 Positioning

Determination of the three-dimensional coordinates of the camera exposure station at the time an image was taken is an important component of any photogrammetric survey. Determination of the three-dimensional coordinates of the camera exposure stations, in the past, was primarily done by a method known as photo triangulation. Photo triangulation is a method in which intersection points of the same object in different images, with known three-dimensional coordinates, are used in a computational process to derive the position and orientation of the images at the time in which the image was taken by the camera. This method required the knowledge of ground control points (points with known 3D coordinates) in a set of overlapping images.

More recently, the Navstar Global Positioning System (GPS), "has become generally available and has been considered fully operational on a worldwide basis since 1993." (Ebadi, pg 6, 1997) The development of the Global Positioning System has allowed for a much easier way to determine the exterior orientation parameters (position and orientation) of the camera exposure stations at the time of exposure. In aerial applications, the airborne kinematic GPS method has been used to determine these exterior orientation parameters each time an image is taken. In kinematic GPS, "the rover station is in constant motion ... [and] requires a stationary receiver to be located at a known base station, and an initial start-up period during which the rover receiver is held stationary."(Wolf et al, 2000). The purpose of including a "start-up" time is so that integer ambiguities can be calculated by software applications. After the unknown integer ambiguities have been determined, the rover station can then begin moving. However, this can only continue as long as a constant lock is maintained on the satellites. If, as in the case of mobile mapping applications, there occurs a loss of signal lock due to the receiver onboard the mobile platform passing under a tree or bridge, or via some other obstructions, then the rover station must return to a previously surveyed position. This major disadvantage limits the use of kinematic GPS methods to areas in which there are little to no obstructions; primarily areas considered "open areas". To overcome this drawback, a method was developed known as on-the-fly ambiguity resolution. "This method of ambiguity resolution is performed by a software technique whereby many trial combinations of integer ambiguities for the different satellites are tested in order to determine the correct set." (Wolf et al, pg 361, 2000).

The advent of the Global Positioning System has greatly enhanced the ability of exterior orientation determination of camera exposure stations in photogrammetric applications, both in airborne and land-based mapping. Ebadi (1997) has concluded that the use of the global positioning system has also helped in achieving greater accuracy of exterior orientation parameters by including the GPS measurements into the aerial triangulation adjustment. “The combined GPS-photogrammetric block adjustment takes advantage of weighted GPS observations, which significantly reduces the number of ground control points needed in a conventional block adjustment.” (Ebadi, 1997).

1.2.3 Orientation

When taking photographs during a photogrammetric survey, it is always desirable to have the optical axis of the camera to be vertical to the surface being imaged. However, despite great efforts to achieve this goal via, for example in aerial photogrammetry, the use of leveling instruments such as level vials, as well as the use of other stabilization equipment, it is usually not the case that the optical axis will be vertical to the surface being imaged. When the optical axis is not vertical to the surface, the resulting photographs are called tilted photographs. The angular orientation of the photographs at time of exposure is given by three parameters denoted *omega* (ω), *phi* (ϕ), and *kappa* (κ). Figure 1.1 illustrates these three angles:

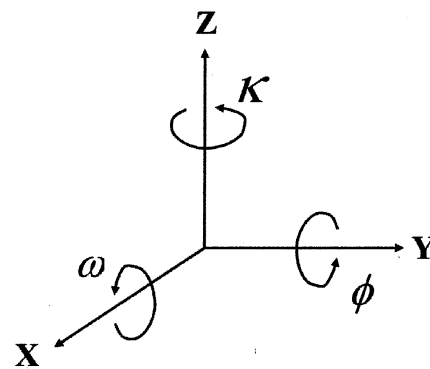


Fig 1.1. Angular orientation parameters. Image provided by Robert Pless, Associate Professor, Washington University

In the above figure, rotation about the x-axis (ω) is known as pitch, rotation about the y-axis (ϕ) is known as roll and rotation about the z-axis (κ) is known as yaw/heading.

In the past, several methods existed to determine the angular orientation of the camera exposure station. One such method was the horizon camera. The horizon camera operates by

taking photographs of the horizon and yields the rotation angles of the camera frame with respect to the horizon. Another method used to determine the angular orientation was the solar periscope. However, the angles determined were referenced to the sun. Both of these methods were considered impractical due to the achievable accuracy falling short of requirements. Today, the approach taken to determine the angular orientation of the exposure station is through the use of an Inertial Measurement Unit (IMU). These IMUs operate by using accelerometers, as well as rate gyroscopes, to sense and detect how the platform on which it is mounted on is rotating in space. Once this is known, position and velocity can be determined by performing integration on the accelerometers and gyros. This is done through the use of an Inertial Navigation System (INS). An INS typically consists of a computer and an IMU, and is initially fed its' position and velocity information from a GPS. It can then use information from its' IMU to compute position and velocity information.

1.2.4 Full-system Integration

Advances in sensors, positioning and orientation have allowed for the potential to combine all of these technologies into a powerful mapping system that can be used to image an area and produce the precise location and orientation of these cameras in a near instantaneous time frame. In particular, the combination of GPS and INS has resulted in a very convenient method of determining position and orientation together. “Since both sensor systems [GPS and INS] are of almost complimentary error behaviour, the ideal combination will provide not only higher positioning, velocity and attitude accuracy but also a significant increase in reliability, as both systems are supporting each other.” (Cramer et al, pg 2, 2001). When there is a loss of signal lock with the GPS system, the INS can help the situation by supplying very accurate information about the initial position, as well as the velocity of the platform, providing ‘trajectory’ information about the platform. In addition to these benefits, the GPS can also assist the INS by providing, “accurate estimates on the current behaviour of its error statistics.” (Cramer et al, pg 2, 2001).

With respect to the imaging sensor (camera) used onboard the platform to map the area of interest, the benefits of an onboard integrated GPS/INS system becomes increasingly apparent. “The direct measurement of the fully exterior orientation of any sensor during data recording becomes feasible [due to the inclusion of an integrated GPS/INS], which offers an interesting alternative to the standard indirect approach of image orientation based on classical aerial

triangulation.” (Cramer, pg 2, 2001). However, due to the fact that the GPS/INS system is physically separated from the imaging sensor, there exist several offsets that must be determined in order to properly identify the final positioning information of the imaging sensor’s perspective center. The diagram below from El-Sheimy (1996) illustrates the relationship between the GPS, INS and camera frames (c-frame).

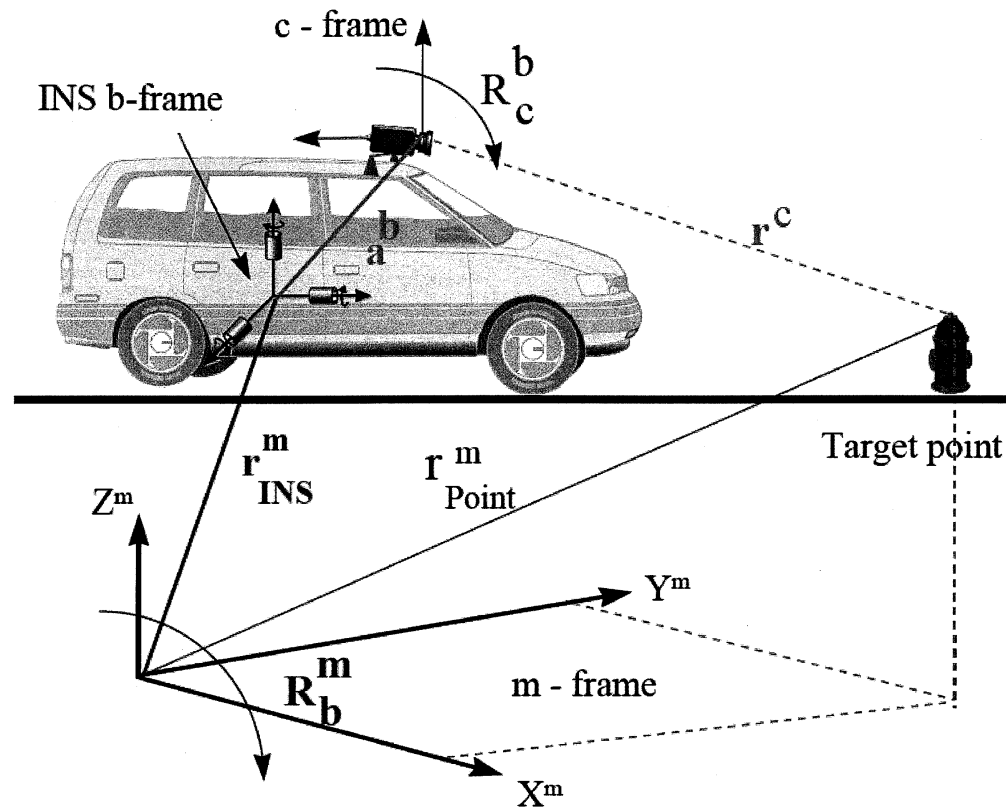


Fig 1.2. Detailed diagram of elements of georeferencing for the close-range case (El-Sheimy, pg 57, 1996).

In Figure 1.2, the offsets that must be determined between the sensor systems is the vector a^b , which is the offset vector between the INS body frame and the camera frame, and R_c^b which is the rotation between the camera’s frame and the INS body frame. Both of these parameters are determined via calibration and will be discussed in later sections. The determination of these parameters provide for the opportunity to relate the coordinates of an object point in the camera frame to its’ corresponding three-dimensional coordinates in an Earth-fixed frame. This will be discussed in later sections.

1.3 Research Objectives

The transportation departments belonging to respective provinces currently collect highway management data with the use of several methods and systems which include a visual field inspection, survey methods, aerial photogrammetry, as well as mobile data acquisition systems. With respect to the mobile acquisition systems, many departments own their own system or rent these systems so as to acquire the highway inventory data which they seek. The benefit of these mobile systems is that they have the ability to capture and record assets belonging to the highway, as well as road conditions of the highway. All of this can be done at a normal highway speed so as to provide the most convenient method of data collection. In addition to these benefits, these mobile systems can also record the three-dimensional coordinates of lanes and centerlines, as well as appurtenances, panoramic right-of-way video and pavement video. Many systems operate through the use of a series of cameras which record images of the surroundings and derive information of interest from these images. If, instead of using standard cameras, the inclusion of a spherical camera was used in conjunction with these systems, the generation of high precision-three dimensional coordinate information can be derived for the parameters of interest on a highway with complete coverage. The desired information can then be georeferenced and can then be entered into highway management systems to provide a much more convenient and efficient method of field crew deployment for maintenance and upkeep of a highway.

All information collected by mobile mapping systems requires a method of georeferencing this information so that it can be related to an Earth-fixed coordinate frame. Georeferencing essentially refers to the process of assigning three-dimensional coordinates to points in an image. Prior to the georeferencing process, these mobile systems also require the determination of a variety of parameters inherent to the camera, and the camera’s spatial location at the time of exposure. The first set of parameters is known as interior orientation parameters, and the second set of parameters are known as exterior orientation parameters. This research paper will extend current methods of determination of these parameters to the application of a spherical camera. For the purposes of this paper, a series of computer programs were written and, collectively, they provide a means of determining the following:

- Interior orientation of each camera which comprise the spherical camera,
- Relative orientation existing between each camera of the spherical camera body,

- Position and orientation of each camera at time of exposure

In addition to these programs, this research paper will propose a method of “stitching” each image captured by the spherical camera to build a 360-degree panoramic, “immersive” image strip. Achieving accurate color and tonal balance across the image will also be discussed. Finally, the determination of the positional offset vector between each camera perspective center and the GPS mounted on the vehicle, as well as the orientation offset between each camera and the IMU will also be discussed.

2. Collinearity Equation

Before a discussion on the determination of the interior and exterior orientation parameters can commence, the collinearity equation must be introduced. The fundamental equation utilized in photogrammetry is known as the collinearity equation. This equation essentially states that, “an object point, its homologous image point, and the perspective centre are all collinear” (Ebadi, pg. 12, 1997). This condition is shown in Figure 2.1, and is followed by the collinear equations themselves.

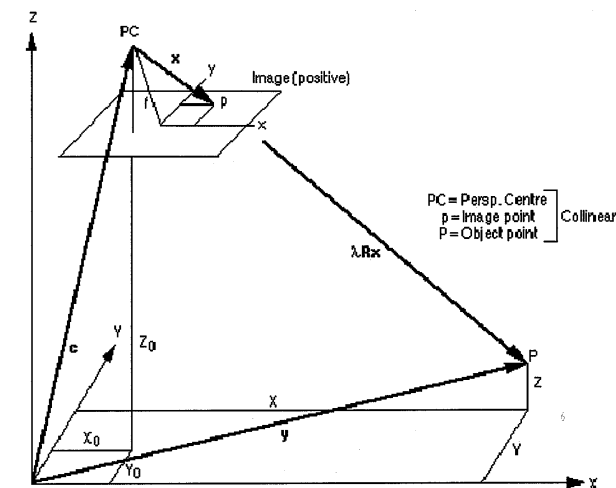


Fig 2.1 Principle of Collinearity Equations.

Image provided by Geometric Software

Collinearity Equations (From Ebadi, 1997)

$$\begin{aligned}
 F_x &= x_i - x_p + c \frac{m_{11}(X_i - X_o) + m_{12}(Y_i - Y_o) + m_{13}(Z_i - Z_o)}{m_{31}(X_i - X_o) + m_{32}(Y_i - Y_o) + m_{33}(Z_i - Z_o)} = 0 \\
 F_y &= y_i - y_p + c \frac{m_{21}(X_i - X_o) + m_{22}(Y_i - Y_o) + m_{23}(Z_i - Z_o)}{m_{31}(X_i - X_o) + m_{32}(Y_i - Y_o) + m_{33}(Z_i - Z_o)} = 0
 \end{aligned}
 \tag{2.1}$$

Where

$$M = M_{\kappa} M_{\phi} M_{\omega} = \begin{bmatrix} m_{11} & m_{12} & m_{13} \\ m_{21} & m_{22} & m_{23} \\ m_{31} & m_{32} & m_{33} \end{bmatrix} = \quad (2.2)$$

$$\begin{bmatrix} \cos(\Phi)\cos(\kappa) & \cos(\omega)\cos(\kappa)+\sin(\omega)\sin(\Phi)\cos(\kappa) & \sin(\omega)\sin(\kappa)-\cos(\omega)\sin(\Phi)\cos(\kappa) \\ -\cos(\Phi)\sin(\kappa) & \cos(\omega)\cos(\kappa)-\sin(\omega)\sin(\Phi)\sin(\kappa) & \sin(\omega)\cos(\kappa)+\cos(\omega)\sin(\Phi)\sin(\kappa) \\ \sin(\Phi) & -\sin(\omega)\cos(\Phi) & \cos(\omega)\cos(\Phi) \end{bmatrix} \quad (2.3)$$

Where:

(x_i, y_i) = the image coordinates,

(x_p, y_p) = coordinates of the principal point,

c = the camera constant,

m_{ij} = elements of the 3D rotation matrix,

(X_i, Y_i, Z_i) = coordinates of the object points,

(X_o, Y_o, Z_o) = coordinates of the exposure station,

M = rotation matrix,

(ω, ϕ, κ) = rotation angles, (change Φ in rotation matrix (2.2) to ϕ)

k_y = the scale factor corresponding to the y axis in digital camera.

The determination of the interior and exterior orientation parameters in a photogrammetric survey is often performed by solving the collinearity equations for each of these parameters by means of a least-squares adjustment. Details on this will be explored in later sections.

3. Camera Calibration

3.1 Immersive Media Dodecahedron Camera

The spherical camera considered as the sensor for the mobile mapping platform proposed in this project is the Dodeca 2360 Camera, manufactured by Immersive Media Corporation. The body of the camera is in the shape of a dodecahedron, “a platonic solid composed of twelve regular pentagonal faces, with three faces meeting at each vertex.” (Wikipedia) Below is a figure of a typical dodecahedron :

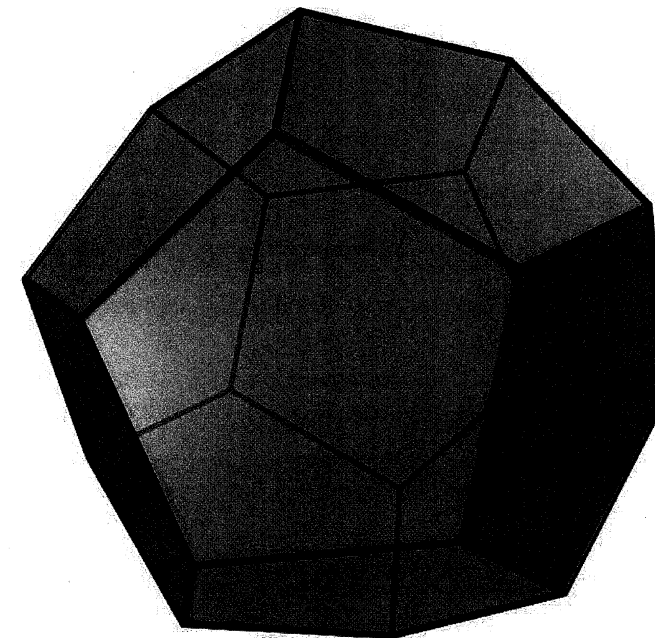


Fig 3.1 Image provided by Wikimedia

Given below is a figure of the Dodeca 2360 by Immersive Media.



Fig 3.2 - Dodeca 2360 – Image Provided by Immersive Media

The Dodeca 2360 consists of the following (information provided by Immersive Media)

- Eleven CCD 1/3” sensors in a modular dodecahedral array
- Field of view of full array: 360 degrees horizontal, 290 degrees vertical (91.7% of sphere)
- Most efficient division of the sphere for consistent quality in all directions

In order to properly utilize the Dodeca 2360 camera system for use in a mobile mapping system, the determination of the relative orientation (offset and angular differences) between each “face” or camera of the dodecahedron must be determined, as well as the interior orientation of each camera. Furthermore, the offset vector between each camera and the GPS, as well as the angular differences between each camera and the INS must also be determined. Determination of the relative orientation between each camera of the dodecahedron, as well as the interior orientation parameters, will be discussed herein. The determination of the offset

vectors and angular differences between the cameras and the GPS/INS components will be discussed in later sections.

3.2 Interior Orientation Parameters

Interior orientation parameters are the elements which define the interior geometry of any standard metric or digital camera. The calibration of a camera to determine these parameters is a process which must be performed prior to any photogrammetric survey. There are four components to interior orientation parameters. These are listed below:

- The principal point coordinates (x_p, y_p) ,
- The focal length of the lens f ,
- The scale factor corresponding to the y-axis,
- Lens distortion parameters (5 parameters).

For the purposes of this project, the interior orientation parameters for each camera of the IMC camera must be solved for. In order to solve for these parameters, a self-calibrating bundle adjustment must be utilized. The result of the self-calibrating bundle adjustment gives the interior orientation parameters, as well as the spatial coordinates of the camera exposure station (X_o, Y_o, Z_o) and the orientation of the camera at the time of exposure, denoted by (ω, ϕ, κ) (Exterior Orientation Parameters). The self-calibrating bundle adjustment will be discussed in later sections.

3.2.1 Principal Point Coordinate and Scale Factor Determination

The principal point is the point in the image which is considered the geometric centre of the image. In the aerial photography case, this point coincides with the point on the ground in which the optical axis intersects. The principal point, as well as the scale factor, k_y , relate the image coordinate system to the computer coordinate system. The scale factor k_y accounts for the y-axis scale factor as well as a reflection of (-1) to take into consideration the difference in the image coordinate system and the computer coordinate system (one is a right handed system and the other is left handed). The transformation from the computer coordinate system to the image coordinate system is given below from El-Sheimy (1996) below:

$$\bar{x} = x_c - x_p, \quad (3.1)$$

$$\bar{y} = (y_c - y_p) / k_y \quad (3.2)$$

Where:

- (x_p, y_p) are the principal point coordinates,
- (\bar{x}, \bar{y}) are the image coordinates,
- (x_c, y_c) are the computer coordinates,
- k_y is the scale factor corresponding to the y-axis.

The determination of the principal point coordinates and the scale factor is done via a self-calibrating bundle adjustment. This bundle adjustment makes use of the collinearity Equations 2.1 given previously. These equations are reproduced below for reference, and are slightly modified in appearance to reflect the parameters of interest which are sought after:

$$x_i = -f \frac{U}{W} + \Delta x, \quad (3.3)$$

$$y_i = -f \frac{V}{W} + \Delta y. \quad (3.4)$$

Where:

- $U = U = m_{11}(X_i - X_o) + m_{12}(Y_i - Y_o) + m_{13}(Z_i - Z_o)$,
- $V = V = m_{21}(X_i - X_o) + m_{22}(Y_i - Y_o) + m_{23}(Z_i - Z_o)$,
- $W = W = m_{31}(X_i - X_o) + m_{32}(Y_i - Y_o) + m_{33}(Z_i - Z_o)$,
- f = focal length of the lens,
- Δx and Δy are correction terms corresponding primarily to the lens distortion inherent to each camera,

3.2.2 Lens Distortion Parameters Determination

Lens distortions are caused by imperfections in the manufacturing of the lens, and result in incoming light rays being bent and changing directions after passing through the lens in such a way that their direction of travel is no longer parallel to their incoming directions. They do not degrade the image quality, but they do degrade the geometric quality of the images. Two types of lens distortions which are normally prevalent are the symmetric radial lens distortions as well as decentering lens distortions. In symmetric radial lens distortion, imaged points become distorted along radial lines which emanate from the optical axis. Decentering lens distortions

causes off-center patterns of distortion. The mathematical models used to model these distortions are given below from El-Sheimy (1996);

$$\Delta x = x_i(k_1 r^2 + k_2 r^4 + k_3 r^6) + p_1(r^2 + 2x_i^2) + 2p_2 x_i y_i \quad (3.5)$$

$$\Delta y = y_i(k_1 r^2 + k_2 r^4 + k_3 r^6) + 2p_1 x_i y_i + p_2(r^2 + 2y_i^2) \quad (3.6)$$

Where:

- k_1, k_2, k_3 are related to the symmetric radial distortion,
- p_1, p_2 are related to the decentering tangential distortion,
- $r = \sqrt{\bar{x}_i^2 + \bar{y}_i^2}$.

3.3 Relative Orientation Determination

As was mentioned earlier, the determination of the offset vector(s) between each face of the dodecahedron must be determined, as well as the angular differences between each face. In order to determine these parameters, a simple “unit” pentagon is considered (i.e., the length of each side is 1)

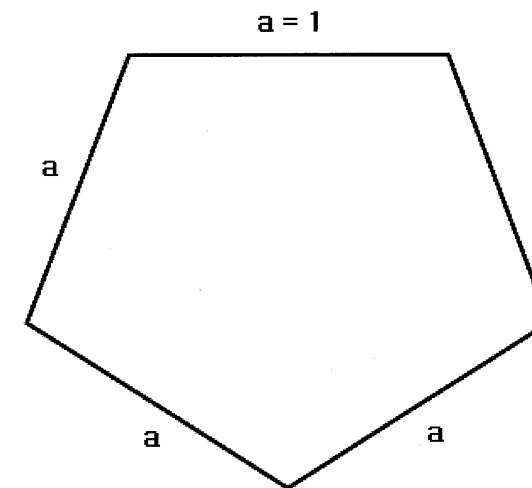


Fig 3.3 - Regular Pentagon – Side Length = 1

In order to determine the relative orientation existing between each pentagonal face of the dodecahedron, the vertices of the pentagon given above must be determined. This is done by

first superimposing a local 2-D coordinate frame on the above pentagon, centered at the centroid.

This is shown below

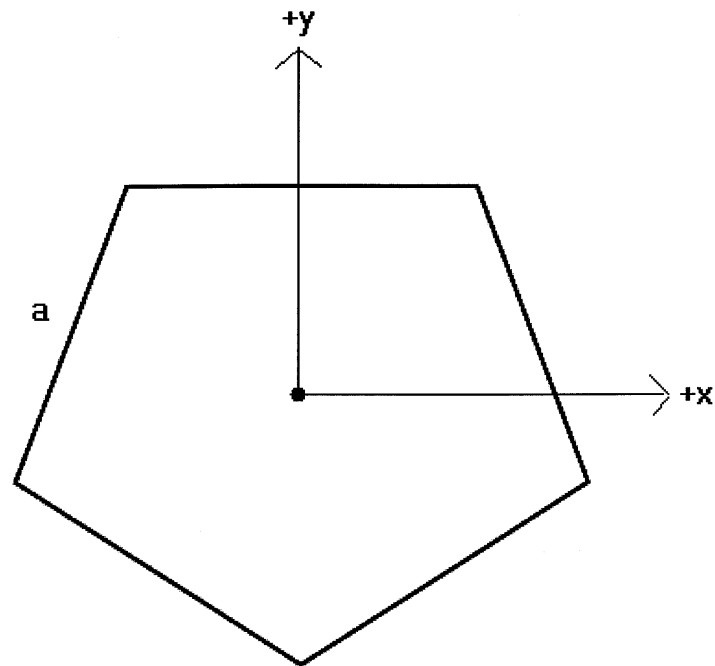


Fig 3.4 - Regular Pentagon with Local 2-D Coordinate Frame Superimposed

To compute the coordinates of the vertices, some well-known mathematical relationships for a regular pentagon must be utilized. These are illustrated below:

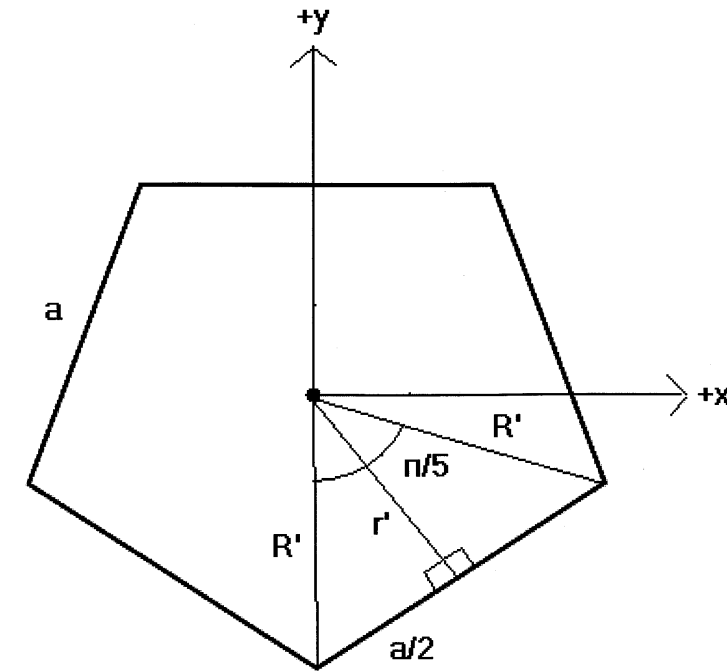


Fig 3.5 - Mathematical relationships of a regular pentagon

Where:

$$\bullet R' = \frac{1}{10} a \sqrt{50 + 10\sqrt{5}} \quad (3.7)$$

$$\bullet r' = \frac{1}{10} a \sqrt{25 + 10\sqrt{5}} \quad (3.8)$$

With these equations in hand, and knowing that the interior angles of a pentagon are 108 degrees, the following vertices were computed:

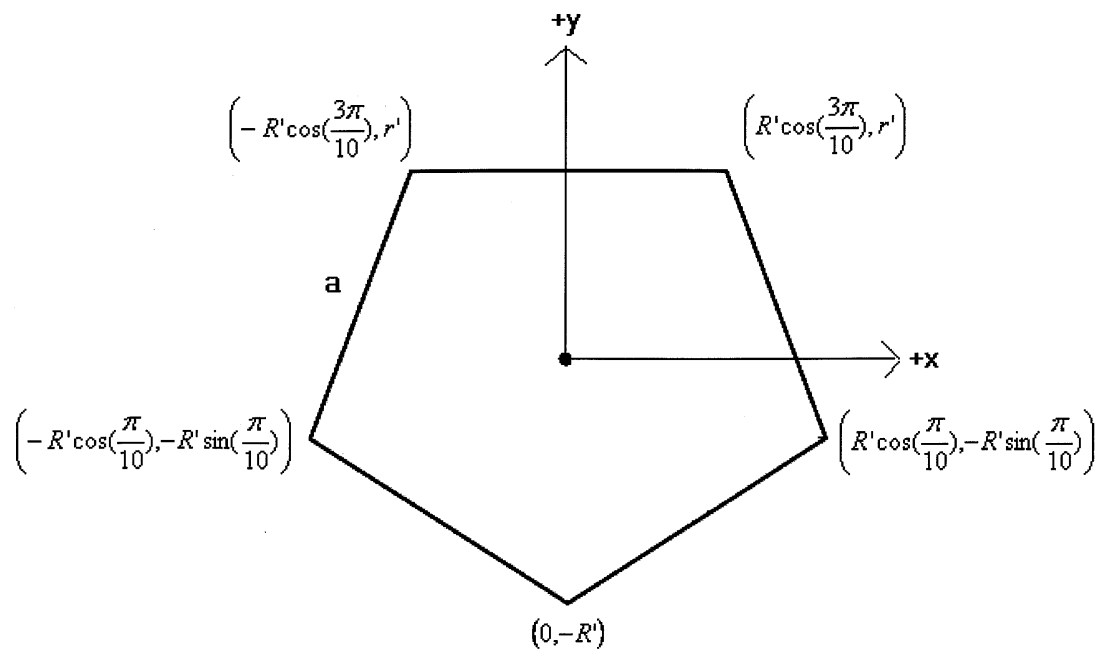


Fig 3.6 - Vertices of a Regular Pentagon

Once the vertices of the regular pentagon have been determined, it now becomes possible to determine the coordinates of the vertices of every other pentagonal face of the dodecahedron. This can be done by first introducing the Z-Axis to our already established coordinate system. The positive Z-Axis points out of the page, and completes the right-handed coordinate system. Next, the pentagon given above is designated as the “top” face of the dodecahedron. This gives a dodecahedron whose coordinate system is centered on the top face.

To compute the coordinates of the vertices of each pentagonal face of the dodecahedron with respect to the coordinate frame centered on the top face, the knowledge of the dihedral angle of a dodecahedron is utilized. The dihedral angle is the angle between any two adjacent faces of a polyhedron. In the case of a dodecahedron, this angle is approximately 116 degrees. Next, the coordinates of the vertices of the top face about the x, y and z axes are rotated by various angles, and then translate these coordinates so as to obtain the coordinates of the vertices of the pentagonal faces of the upper portion of the dodecahedron. Rotation angles about the Z-Axis are derived using geometric knowledge of a pentagon, whereas rotations about the X/Y-Axes are derived from knowledge of the dihedral angle. An example is given below for the determination of the vertices of one of the faces. First, a translation is applied to the points such

that vertex V4 (shown in Figure 3.7) becomes centered at the origin (this is done by subtracting the coordinates of V4 from all the other vertices). The vertices are then rotated about the X-Axis by +64 degrees, and then rotated about the Z-Axis by +108 degrees. This gives the following diagram (note that this is 2-D, so the effect of depth is not shown). The rotated pentagonal face is angled “downward” (into page) by 64 degrees.

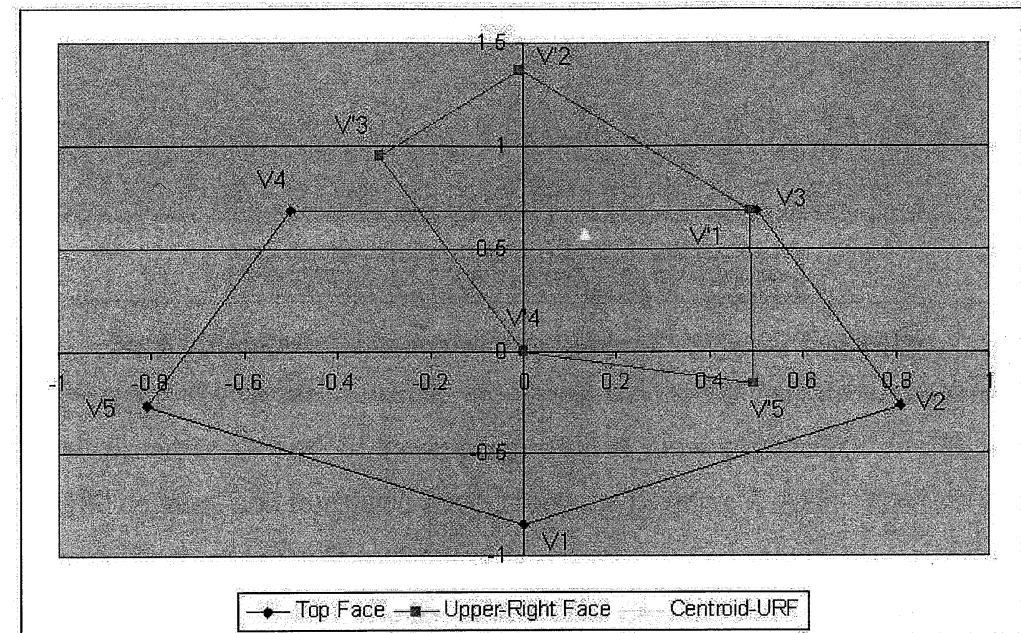


Fig 3.7 - Pentagon with V4 Centered on Origin, followed by rotation of 64 Degrees about X Axis, followed by another rotation of 108 degrees about the Z-Axis

The rotated pentagon is then translated in such a way so as to align edge V'4-V'3 to edge V2-V3. This is done by adding the coordinates of vertex V2 to all of the V' coordinates. This gives the following figure:

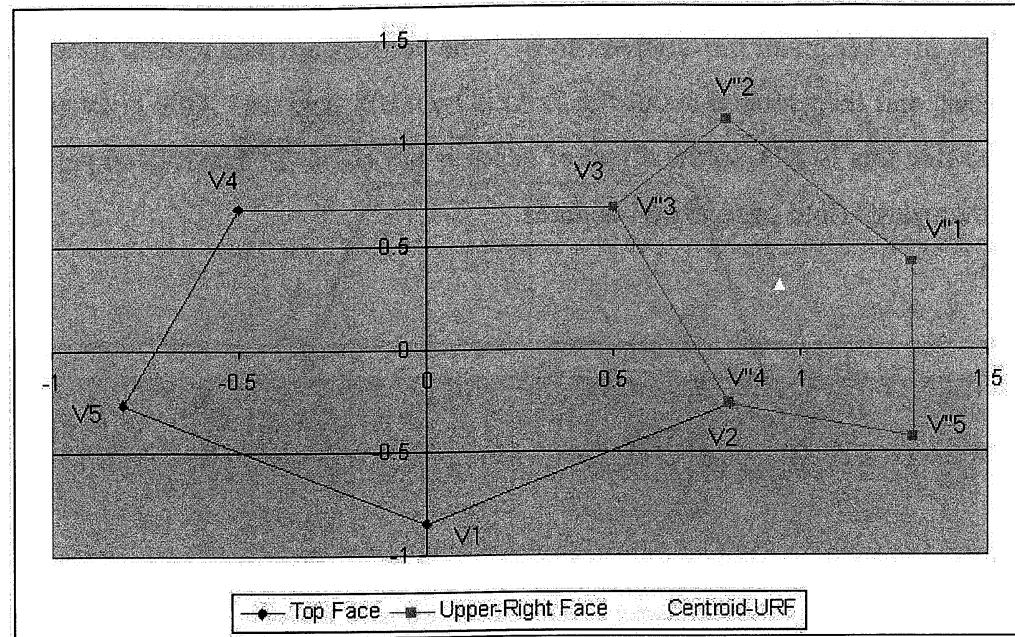


Fig 3.8 – Upper Right Face of Dodecahedron with Reference Top Face

The equation used to calculate the coordinates of the vertices of the new face is given below:

$$\begin{bmatrix} X \\ Y \\ Z \end{bmatrix}_{V''} = \begin{bmatrix} X \\ Y \\ Z \end{bmatrix}_{V2} + R_z(108^\circ)R_x(64^\circ) \begin{bmatrix} X - V4_x \\ Y - V4_y \\ Z - V4_z \end{bmatrix} \quad (3.9)$$

Where:

$$R_z(\vartheta) = \begin{bmatrix} \cos(\vartheta) & -\sin(\vartheta) & 0 \\ \sin(\vartheta) & \cos(\vartheta) & 0 \\ 0 & 0 & 1 \end{bmatrix} \quad R_x(\vartheta) = \begin{bmatrix} 1 & 0 & 0 \\ 0 & \cos(\vartheta) & -\sin(\vartheta) \\ 0 & \sin(\vartheta) & \cos(\vartheta) \end{bmatrix} \quad (3.10)$$

A similar procedure is performed to compute the coordinates of the vertices of all the other pentagonal faces on the upper portion of the dodecahedron. Figure 3.9 below shows the pentagonal faces plotted in Microsoft Excel for the upper portion of the dodecahedron.

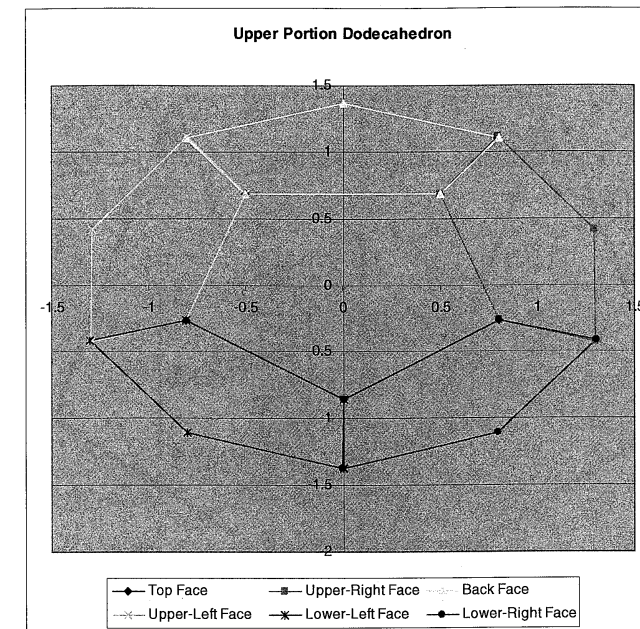


Fig 3.9 – Complete 2D representation of Upper Portion of Dodecahedron

To compute the coordinates of the vertices of the pentagonal faces on the lower portion of the dodecahedron, the vertices of the upper portion of the dodecahedron are rotated about the X-Axis by +180 degrees, and translated down along the negative Z-Axis. The bottom portion of the dodecahedron is given in the Figure 3.10:

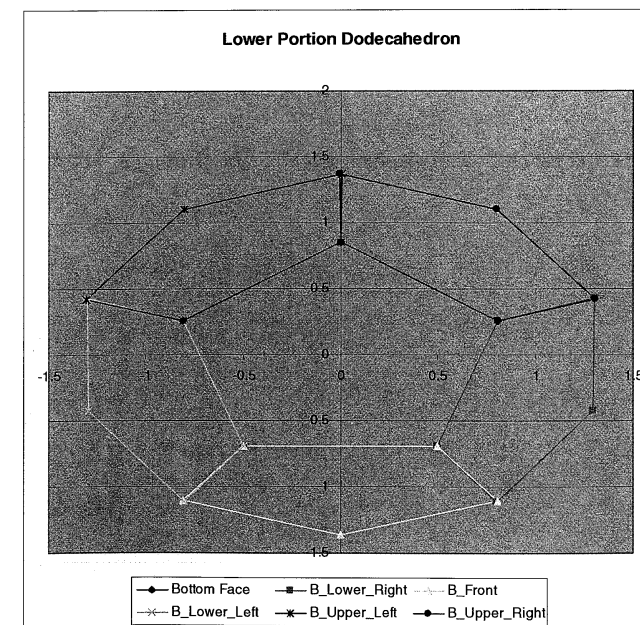


Fig 3.10 – Complete 2D Representation of Lower Portion of Dodecahedron

Once the coordinates of the vertices have been computed, the centroids of each pentagonal face can also be computed. The reason that the positions of the centroids are required is because the centroid is essentially the position of the perspective centre of the camera on the respective faces of the dodecahedron. The equation for the computation of a centroid for a particular face is given below:

$$\begin{bmatrix} X \\ Y \\ Z \end{bmatrix}_{Centroid} = \begin{bmatrix} (\sum_{V1}^{V5} Vx)/5 \\ (\sum_{V1}^{V5} Vy)/5 \\ (\sum_{V1}^{V5} Vz)/5 \end{bmatrix}_{Face1} \quad (3.11)$$

The centroids essentially provide the offset vectors between perspective centers of each camera. Together with the rotation angles used to rotate the reference face, a complete set of relative orientation parameters are obtained. As a final check to ensure that the rotation angles utilized are correct, the orientation of the local reference frame of each individual pentagonal face is computed as follows:

For each face:

- 1) Compute Vectors V3V1 and Vectors V4V1, then compute the bi-sector of these two vectors. Normalize the bi-sector to obtain direction vector of the Y-Axis:

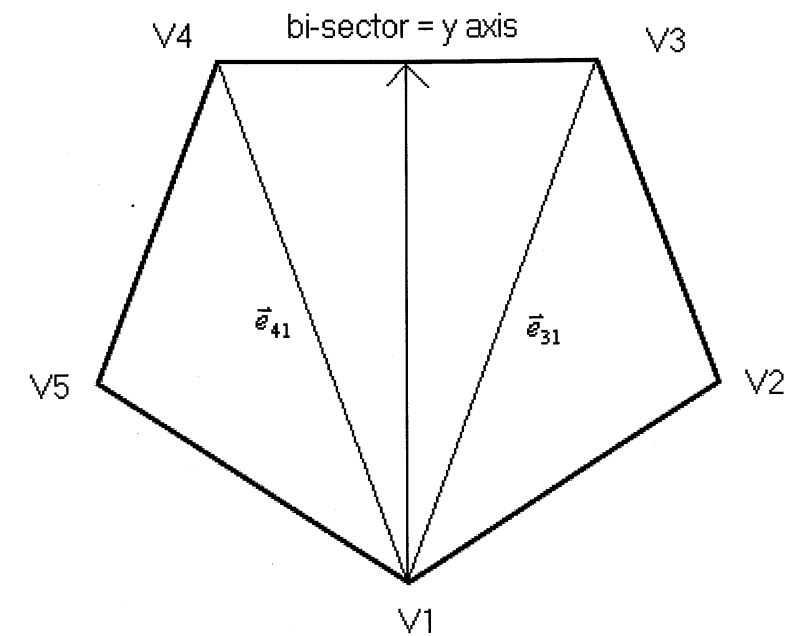


Fig 3.11 – Compute Vectors V3V1, V4V1 and Bi-Sector

$$\vec{e}_{41} = \begin{bmatrix} X_4 - X_1 \\ Y_4 - Y_1 \\ Z_4 - Z_1 \end{bmatrix} \quad \vec{e}_{31} = \begin{bmatrix} X_3 - X_1 \\ Y_3 - Y_1 \\ Z_3 - Z_1 \end{bmatrix} \quad bi\text{-sector} = \vec{e}_{41} + \vec{e}_{31} \quad (3.12, 3.13, 3.14)$$

$$Yaxis\text{-direction} = \text{normalize}(bi\text{-sector}) \quad (3.15)$$

- 2) Take the cross-product of \vec{e}_{41} and \vec{e}_{31} , then normalize to obtain the direction vector for the Z-Axis:

$$Zaxis\text{-direction} = \text{normalize}(\vec{e}_{41} \times \vec{e}_{31}) \quad (3.16)$$

- 3) Take the cross-product of the Y-axis Direction vector with the Z-axis Direction vector to obtain the X-axis Direction:

$$Xaxis\text{-direction} = Yaxis \times Zaxis \quad (3.17)$$

4) With the direction of each axis defined, the following matrix can be formed

$$\vec{e}_{LF} = \begin{bmatrix} e_{x_x} & e_{y_x} & e_{z_x} \\ e_{x_y} & e_{y_y} & e_{z_y} \\ e_{x_z} & e_{y_z} & e_{z_z} \end{bmatrix} \quad (3.18)$$

Where \vec{e}_{LF} describes the orientation of each axis on the local face, and each column in the above matrix is the direction vector for the x-axis, y-axis, and z-axis, respectively.

5) To check the rotation angles and ensure they are correct, the rotation matrix that rotates the coordinate frame of the top face to the coordinate frame of the face under investigation must be determined. This is done by forming the following relationship:

$$\vec{e}_{LF} = R \cdot \vec{e}_{TF} \quad (3.19)$$

Where:

- \vec{e}_{TF} is the orientation of the coordinate frame of the top face (our reference face) and is simply given as follows:

$$\vec{e}_{TF} = \begin{bmatrix} 1 & 0 & 0 \\ 0 & 1 & 0 \\ 0 & 0 & 1 \end{bmatrix} \quad (3.20)$$

- R is the combined rotation matrix resulting from the consecutive rotations of $R_x(\omega) \cdot R_y(\phi) \cdot R_z(\kappa)$ and is given below:

$$R = \begin{bmatrix} \cos\phi\cos\kappa & \cos\phi\sin\kappa & -\sin\phi \\ -\cos\omega\sin\kappa + \sin\omega\sin\phi\cos\kappa & \cos\omega\cos\kappa + \sin\omega\sin\phi\sin\kappa & \sin\omega\cos\phi \\ \sin\omega\sin\kappa + \cos\omega\sin\phi\cos\kappa & -\sin\omega\cos\kappa + \cos\omega\sin\phi\sin\kappa & \cos\omega\cos\phi \end{bmatrix} \quad (3.21)$$

Since \vec{e}_{LF} is known, and \vec{e}_{TF} is known, one must only solve for the elements of R. This is simplified further by the fact that \vec{e}_{TF} is identity. This gives the following:

$$\vec{e}_{LF} = R \quad (3.22)$$

Solving for the rotation angles is therefore given as follows:

$$\phi = \sin^{-1}(e_{x_x}) \quad (3.23)$$

$$\kappa = \tan^{-1}\left(\frac{e_{y_x}}{e_{x_x}}\right) \quad (3.24)$$

$$\omega = \tan^{-1}\left(\frac{e_{x_y}}{e_{x_z}}\right) \quad (3.25)$$

These angles were computed for each face and were equivalent to the angles used to initially rotate the coordinates of the vertices of the reference face.

Each face was assigned a "camera" number. In Table 3.1, each camera number is given with its offset and orientation. Prior to this, the location of the reference frame was translated downwards from the top face to the centre of the dodecahedron to simplify the situation.

CAMERA NUM	X(m)	Y(m)	Z(m)	Kappa(deg)	Phi(deg)	Omega(deg)
1000	0.000	0.000	1.119	0	0	0
1001	0.941	0.306	0.500	108	0	64
1002	0.000	0.990	0.500	180	0	64
1003	-0.941	0.306	0.500	-108	0	64
1004	-0.582	-0.801	0.500	-36	0	64
1005	0.582	-0.801	0.500	36	0	64
1006	0.000	0.000	-1.119	0	0	180
1007	0.941	-0.306	-0.500	-108	0	-116
1008	0.000	-0.990	-0.500	180	0	-116
1009	-0.941	-0.306	-0.500	108	0	-116
1010	-0.582	0.801	-0.500	36	0	-116
1011	0.582	0.801	-0.500	-36	0	-116

Table 3.1 – List of cameras and their associated position and orientation information

Each pentagonal face was also plotted in Google SketchUp according to edge-length ($a=1$), CCD offset (x, y, z from Table 3.1) and rotation angles (from Table 3.1). The result is given below:

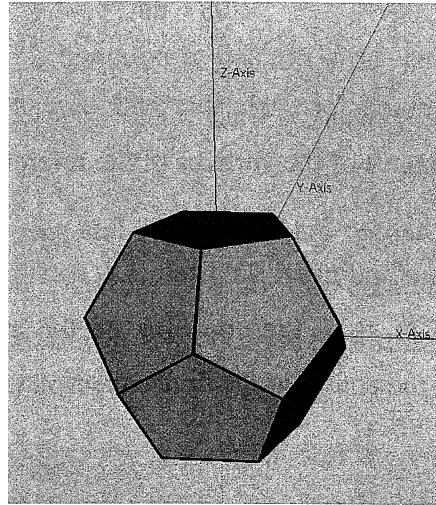


Fig 3.12 – Front view of Dodecahedron

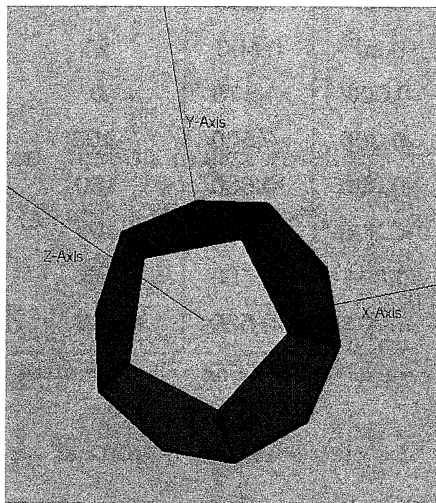


Fig 3.13 – Top view of Dodecahedron

4. Solving for Interior Orientation Parameters

The self-calibrating bundle adjustment was utilized to solve for the interior orientation parameters of each camera of the dodecahedron. The relative orientation parameters determined in Section 3 were used as estimates of the exterior orientation parameters for the model. For the purposes of this research, the method employed is the Normal Equation Formation method of solving the self-calibrating bundle adjustment. The following algorithm was programmed using the Fortran programming language and utilized for a 12 camera, 12 image, 697 point, 804 observation system (see Section 6 for results and observations). For completeness, 12 cameras, resulting in 12 images, is chosen to reflect the entire dodecahedron. In reality, with respect to the actual camera system, this would really be an 11 camera and, therefore, an 11 image system. Ground control points were simulated by generating a series of virtual “spheres”, each centered at the centre of the dodecahedron, and each with varying radii. Each sphere was tessellated using different grid spacing to generate the virtual points. Given below is an example of one of the virtual spheres centered at the center of the dodecahedron.

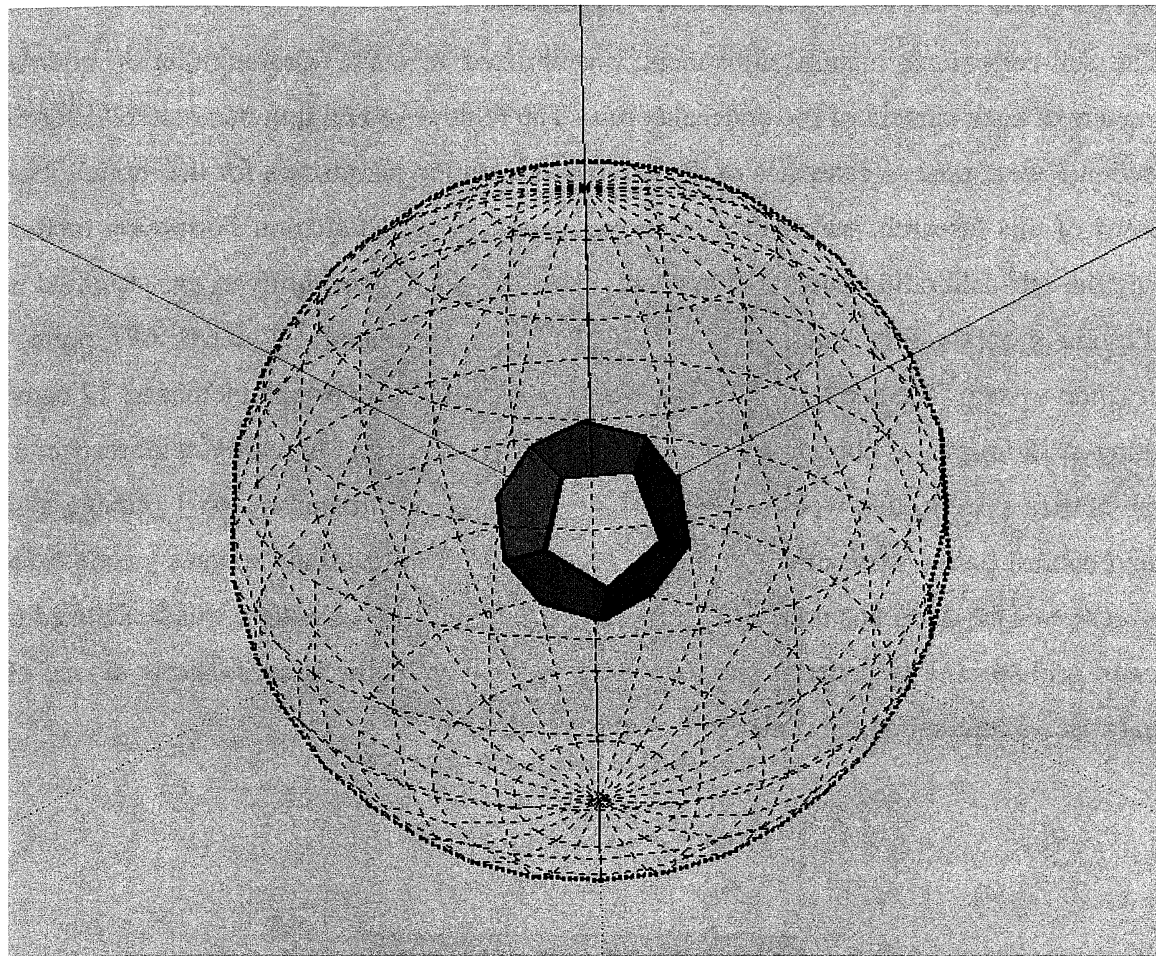


Fig 4.1 – Virtual sphere of points centered at centre of dodecahedron

An assumption was made that the field of view of each camera was 80 degrees and that the format size of the CCD was 640x480. An estimated focal length for each camera was computed using the following equation (provided by Wolfram MathWorld):

$$fov = 2 \tan^{-1} \left(\frac{D}{2f} \right) \quad (4.1)$$

Where:

- fov = field of view = 80 degrees
- D = size of the image sensor (in pixels) = 640 pixels
- f = focal length

Re-arranging Equation 4.1 and solving for focal length, a focal length of 381 pixels is obtained. For each of the virtual points on the sphere, corresponding observation image points were generated for each camera, using the collinearity equations, and the parameters of interior and exterior orientation given below:

CAM	X	Y	Z	κ (deg)	ϕ (deg)	ω (deg)
1000	0.000	0.000	1.119	0.000	0.000	0.000
1001	0.941	0.306	0.500	108.000	0.000	64.000
1002	0.000	0.990	0.500	180.000	0.000	64.000
1003	-0.941	0.306	0.500	-108.000	0.000	64.000
1004	-0.582	-0.801	0.500	-36.000	0.000	64.000
1005	0.582	-0.801	0.500	-36.000	0.000	64.000
1006	0.000	0.000	-1.119	0.000	0.000	180.000
1007	0.941	-0.306	-0.500	-108.000	0.000	-116.000
1008	0.000	-0.990	-0.500	180.000	0.000	-116.000
1009	-0.941	-0.306	-0.500	108.000	0.000	-116.000
1010	-0.582	0.801	-0.500	36.000	0.000	-116.000
1011	0.582	0.801	-0.500	-36.000	0.000	-116.000

Table 4.1 – List of cameras and associated position and orientation information

CAM	F	xp	yp	k1	k2	k3	p1	p2
1000	380.000	2.000	-2.000	-6.11E-08	2.16E-14	3.14E-21	-5.63E-07	2.45E-07
1001	380.000	2.000	-2.000	-6.11E-08	2.16E-14	3.14E-21	-5.63E-07	2.45E-07
1002	380.000	2.000	-2.000	-6.11E-08	2.16E-14	3.14E-21	-5.63E-07	2.45E-07
1003	380.000	2.000	-2.000	-6.11E-08	2.16E-14	3.14E-21	-5.63E-07	2.45E-07
1004	380.000	2.000	-2.000	-6.11E-08	2.16E-14	3.14E-21	-5.63E-07	2.45E-07
1005	380.000	2.000	-2.000	-6.11E-08	2.16E-14	3.14E-21	-5.63E-07	2.45E-07
1006	380.000	2.000	-2.000	-6.11E-08	2.16E-14	3.14E-21	-5.63E-07	2.45E-07
1007	380.000	2.000	-2.000	-6.11E-08	2.16E-14	3.14E-21	-5.63E-07	2.45E-07
1008	380.000	2.000	-2.000	-6.11E-08	2.16E-14	3.14E-21	-5.63E-07	2.45E-07
1009	380.000	2.000	-2.000	-6.11E-08	2.16E-14	3.14E-21	-5.63E-07	2.45E-07
1010	380.000	2.000	-2.000	-6.11E-08	2.16E-14	3.14E-21	-5.63E-07	2.45E-07
1011	380.000	2.000	-2.000	-6.11E-08	2.16E-14	3.14E-21	-5.63E-07	2.45E-07

Table 4.2 – List of cameras and associated interior orientation information

A test was required to ensure that the image points calculated fell within the format of the camera in question. Below is an example of the image coordinate system utilized:

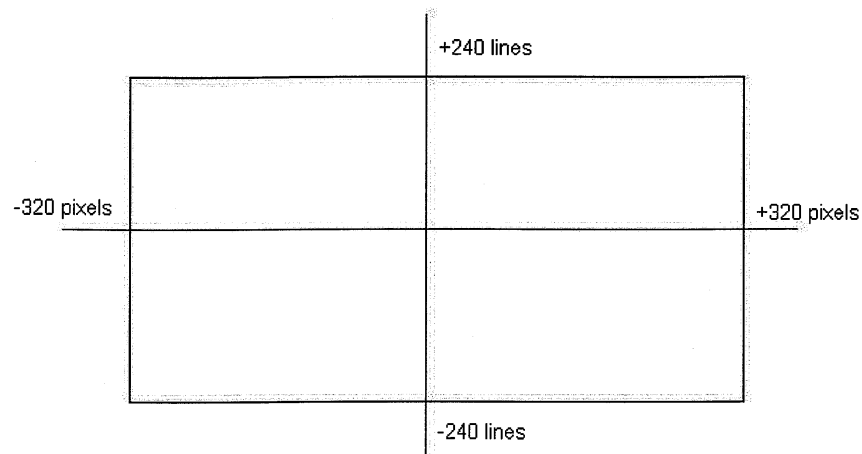


Fig 4.2 – Example image coordinate system utilized

Any image points falling outside of the format size (i.e., $-320px < x < +320$ and $-240ln < y < +240ln$) were considered not to be a point for which the particular camera can see.

Once the observation points for each camera were determined, the self-calibrating bundle adjustment can be solved. This adjustment is solved by first writing out the linearised collinearity equations for each image i and each point j .

$$\underset{2 \times 1}{v_{ij}} + \underset{2 \times 6}{Aeo} \underset{6 \times 1}{dx^{eo}} + \underset{2 \times 3}{As} \underset{3 \times 1}{dx^s} + \underset{2 \times 8}{Aio} \underset{8 \times 1}{dx^{io}} = \underset{2 \times 1}{Wph} \quad (4.2)$$

Where the $\underset{6 \times 1}{dx^{eo}}$ contains the corrections to the exterior orientation parameters of image i , $\underset{3 \times 1}{dx^s}$ contains the corrections to the coordinate of point j and $\underset{8 \times 1}{dx^{io}}$ contains the corrections to the interior orientation parameters of image i , and Aeo , As , and Aio represent partial differential equations of the collinearity Equations 2.1 with respect to exterior orientation parameters, object space coordinates, and interior orientation parameters, respectively. Wph represents the misclosure vector.

The least-squares normal equations associated with one image of one point is then formed as follows:

$$\begin{bmatrix} \underset{l}{Aeo_{ij}^T} \underset{l}{C_{ij}^{ph-1}} & \underset{l}{Aeo_{ij}} & \underset{l}{Aeo_{ij}^T} \underset{l}{C_{ij}^{ph-1}} \underset{l}{As_{ij}} & \underset{l}{Aeo_{ij}^T} \underset{l}{C_{ij}^{ph-1}} & \underset{l}{Aio_{ij}} \\ \underset{l}{As_{ij}^T} \underset{l}{C_{ij}^{ph-1}} & \underset{l}{Aeo_{ij}} & \underset{l}{As_{ij}^T} \underset{l}{C_{ij}^{ph-1}} & \underset{l}{As_{ij}^T} \underset{l}{C_{ij}^{ph-1}} & \underset{l}{Aio_{ij}} \\ \underset{l}{Aio_{ij}^T} \underset{l}{C_{ij}^{ph-1}} & \underset{l}{Aeo_{ij}} & \underset{l}{Aio_{ij}^T} \underset{l}{C_{ij}^{ph-1}} & \underset{l}{Aio_{ij}^T} \underset{l}{C_{ij}^{ph-1}} & \underset{l}{Aio_{ij}} \end{bmatrix} \begin{bmatrix} dx_i^{eo} \\ dx_j^s \\ dx_i^{io} \end{bmatrix} = \begin{bmatrix} \underset{l}{Aeo_{ij}^T} \underset{l}{C_{ij}^{ph-1}} \underset{l}{Wph_{ij}} \\ \underset{l}{As_{ij}^T} \underset{l}{C_{ij}^{ph-1}} \underset{l}{Wph_{ij}} \\ \underset{l}{Aio_{ij}^T} \underset{l}{C_{ij}^{ph-1}} \underset{l}{Wph_{ij}} \end{bmatrix} \quad (4.3)$$

Equation 4.3 can be re-written as follows:

$$\begin{bmatrix} Neo_i & Neo \cdot s_{ij} & Neo \cdot io_i \\ Neo \cdot s_{ij}^T & Ns_j & Ns \cdot io_{ij} \\ Neo \cdot io_i^T & Nio \cdot s_{ij}^T & Nio_i \end{bmatrix} \begin{bmatrix} dx_i^{eo} \\ dx_j^s \\ dx_i^{io} \end{bmatrix} = \begin{bmatrix} teo_i \\ ts_j \\ tio_i \end{bmatrix} \quad (4.4)$$

Where:

- Neo_i contains coefficients of the image parameters
- Ns_j contains coefficients of point coordinates
- Nio_i contains coefficients of camera calibration parameters
- $Neo \cdot s_{ij}$ refers to both coefficients of image parameters and point coordinates
- $Neo \cdot io_i$ refers to both coefficients of image parameters and camera calibration parameters
- $Ns \cdot io_{ij}$ refers to both coefficients of point coordinates and camera calibration parameters

The assumption is then made that errors in each of the point's image coordinates are uncorrelated with any other image coordinates, including other points imaged on the same image and other images of the same point. However, there may be correlation error in x and y coordinates of any single image point. When the assumption is made that the image coordinate errors are uncorrelated, this implies that all systematic errors have been removed.

The assumption stated above essentially means that the total covariance and weight matrices which contain the covariance and the weight information for each and every image coordinate, is block diagonal. Each of the blocks is a 2x2 matrix which correspond to one set of image measurements for one of the points. If the measurements are independent of each other (as is assumed), and that each of the collinearity equations will refer to only one image and one

point, then the result is that one has the ability to add the contributions to the normal equations from each set of collinearity equations. The following observations can thus be made regarding the normal equations formation:

- The total Neo matrix is actually block diagonal. Each of the 6x6 blocks refers to a separate image, and each Neo_i is the sum of the Neo_{ij} sub-matrices, which are assembled from Aeo_{ij} and C_{ij}^{ph-1} from each of the sets of collinearity equations which are referenced to image i .
- Like the total Neo matrix, the total Ns matrix is also block diagonal with 3x3 blocks on the diagonals which are in reference to coordinates of a single point. Like the Neo_i , the Ns_j is assembled from the As_{ij} and C_{ij}^{ph-1} from each of the sets of collinearity equations referenced to point j .
- Again, similar to Neo and Ns , the total Nio matrix is also block diagonal with 8x8 blocks on the diagonals which are in reference to the camera calibration cameras of a single camera. If all images are from a single camera, then the Nio matrix is just 8x8. Nio_i is assembled from the Aio_{ij} and C_{ij}^{ph-1} from each of the sets of collinearity equations referenced to image i .
- For each $Neo \cdot s_{ij}$ sub-matrix, it is the result of the multiplication between Aeo_{ij} , C_{ij}^{ph-1} and As_{ij} from one of the sets of collinearity equations. If a point does not occur on one of the images, then the $Neo \cdot s_{ij}$ submatrix are zero.
- The $Neo \cdot io_i$ and $Ns \cdot io_{ij}$ sub-matrices are assembled in a similar fashion to that of $Neo \cdot s_{ij}$ and for time sake, will be omitted from explanation.

There are numerous advantages of solving the self-calibrating bundle adjustment problem by this method of normal equations formation. The main advantage is that this particular method

saves processing time and storage space. This is because the other method of solving the self-calibrating bundle adjustment would require the formation of the entire A matrix and then solving N by "brute force" multiplication. In real life situations, given a set of photos/images and points, the entire A matrix will contain mainly zero values. This results in vast amounts of storage space being wasted on the storage of zero values. This also results in vast amounts of processing time wasted in multiplying values by zero when forming the N matrix.

The weight matrices corresponding to the exterior orientation parameters, the object space/point parameters and the interior orientation (camera calibration) parameters are added to their particular sub-matrices (Neo_i, Ns_j, Nio_i) once per iteration. As well, the total corrections to the original parameter observations, Weo_i, Ws_j, Wio_i , are multiplied by their corresponding

parameter covariance matrices ($C_i^{eo-1}, C_j^{s-1}, C_i^{io-1}$) and then subtracted from their respective teo_i, ts_j, tio_i vectors.

The results of the self-calibrating bundle adjustment are given below.

CAM	X	Y	Z	κ (deg)	ϕ (deg)	ω (deg)
1000	0.000	0.000	1.119	0.000	0.003	-0.005
1001	0.941	0.306	0.500	108.007	0.002	63.973
1002	0.000	0.990	0.500	179.996	-0.002	64.056
1003	-0.941	0.306	0.500	-108.004	0.000	63.999
1004	-0.582	-0.801	0.500	-35.992	0.002	64.007
1005	0.582	-0.801	0.500	35.999	-0.006	64.008
1006	0.000	0.000	-1.119	0.000	0.000	179.992
1007	0.941	-0.306	-0.500	-108.006	-0.006	-116.008
1008	0.000	-0.990	-0.500	180.004	0.001	-115.987
1009	-0.941	-0.306	-0.500	108.001	0.009	-116.008
1010	-0.582	0.801	-0.500	35.997	-0.005	-116.000
1011	0.582	0.801	-0.500	-35.979	0.009	-115.999

Table 4.3 – List of cameras and associated position and orientation as determined by self-calibrating bundle adjustment.

CAM	f	x _p	y _p	k1	k2	k3	p1	p2
1000	379.668	1.973	-2.015	-6.11E-08	2.16E-14	3.14E-21	-5.63E-07	2.45E-07
1001	379.494	1.998	-2.192	-6.11E-08	2.16E-14	3.14E-21	-5.63E-07	2.45E-07
1002	379.513	2.025	-1.964	-6.11E-08	2.16E-14	3.14E-21	-5.63E-07	2.45E-07
1003	379.516	2.042	-2.119	-6.11E-08	2.16E-14	3.14E-21	-5.63E-07	2.45E-07
1004	379.416	1.986	-1.995	-6.11E-08	2.16E-14	3.14E-21	-5.63E-07	2.45E-07
1005	379.412	2.160	-1.941	-6.11E-08	2.16E-14	3.14E-21	-5.63E-07	2.45E-07
1006	379.505	1.998	-2.058	-6.11E-08	2.16E-14	3.14E-21	-5.63E-07	2.45E-07
1007	379.556	1.972	-2.197	-6.11E-08	2.16E-14	3.14E-21	-5.63E-07	2.45E-07
1008	379.661	2.024	-1.990	-6.11E-08	2.16E-14	3.14E-21	-5.63E-07	2.45E-07
1009	379.553	2.137	-2.196	-6.11E-08	2.16E-14	3.14E-21	-5.63E-07	2.45E-07
1010	379.528	1.999	-1.994	-6.11E-08	2.16E-14	3.14E-21	-5.63E-07	2.45E-07
1011	379.528	2.145	-1.993	-6.11E-08	2.16E-14	3.14E-21	-5.63E-07	2.45E-07

Table 4.4 – List of cameras and associated interior orientation parameters as determined by self-calibrating bundle adjustment

The Normal Equations Structure is given in Appendix A.

5. Direct and Indirect Georeferencing

In order to obtain useful spatial information from the imagery captured by the spherical camera, the imagery captured must be georeferenced. The crucial requirement for the georeferencing process to take place is that the location of the perspective centre of each camera of the spherical camera be known, as well as its' orientation. Various methods exist for determination of these parameters: indirect georeferencing and direct georeferencing. Each of these methods will be discussed herein, and their potential for use in a mobile mapping system will be investigated.

5.1 Indirect Georeferencing

As had been stated previously, in the past photogrammetric surveys required the establishment and presence of ground control points (GCPs). For aerial photogrammetric surveys, for example, "Ground Control Points (GCPs) were the only required source of information for providing the georeferencing parameters and suppressing undesirable error propagation." (El Sheimy, 1996). Ground Control Points are used as input to the bundle adjustment to obtain the exterior orientation parameters for the cameras used in the survey. The requirement for GCPs proved to be a costly and highly restrictive process; that is, it becomes quite expensive to establish GCPs in the survey region, and in many cases it is not possible (or rather, very difficult) to establish GCPs in certain inaccessible areas.

As part of the indirect georeferencing process, "the use of auxiliary position and navigation sensor data" (El Sheimy, 1996) has been utilized in the past to assist in the determination of the exterior orientation of the camera. Examples include the use of gyros, horizon cameras and stascopes (El Sheimy, 1996). However, even including this auxiliary data still does not remove the need for GCPs.

In the close-range photogrammetry case, the problem becomes even more demanding. Establishment of GCPs for a close-range photogrammetric survey (utilizing a system such as that proposed in this research paper) is even more difficult and bothersome. The development of the Global Positioning System (GPS) helped ease this situation tremendously. The inclusion of a GPS system in a photogrammetric survey (aerial or close-range) finally provided the means to directly measure the exterior orientation parameters desired and thus could potentially eliminate the need for GCPs. (Ackerman, 1995). However, limitations to the use of GCPs in a close-range

photogrammetry survey arise when surveys take place in urban areas, where signal loss can frequently occur. When signal loss occurs, and GPS is the only sensor being utilized to provide positioning information, then the accuracy of the survey can plummet. Therefore, a different approach is required to georeference data collected in a close-range photogrammetry survey. This approach was realized once the development of INS occurred. A direct georeferencing process was finally possible.

5.2 Direct Georeferencing

Direct georeferencing provides the means to obtain accurate positioning information during the course of a photogrammetric survey, without the need for GCPs. This is particularly advantageous for close-range photogrammetric surveys such as that discussed in this paper. Direct Georeferencing of a photogrammetric survey can be realized by the inclusion of GPS and INS instruments onboard the survey platform. As was discussed in Section 1.2.4, the presence of GPS and INS concurrently allow for the presence of signal lock to be more forgiving, as the INS can provide trajectory information during the signal loss period, and thus provide very accurate positioning information for data collection sensors (such as the spherical camera) during GPS signal loss in urban areas.

As noted by El Sheimy (1996) the notion of direct georeferencing “is conceptually different from the notion that a block of connected images and sufficient ground control is needed to solve the georeferencing problem”, as was the case of the indirect georeferencing method. Direct georeferencing is a much more flexible option for photogrammetric surveys as imagery captured is not required to be connected (that is, overlapping). As was also alluded to in Section 1.2.4, direct georeferencing methods require the determination of the offset vectors between the GPS unit and the imaging sensor. In addition to this, the orientation differences between the INS and the camera system must also be determined. Orientation differences between the INS body system and the camera body system are known as bore-sight angles. Positional differences between the GPS body system and the camera body system are known as lever arms. Both of these parameters will be discussed in the next section, and methods of determining them will also be examined.

6. Bore-sight and Lever Arm Determination

In order to take advantage of the availability of direct georeferencing in terrestrial mapping applications, the determination of the rotational angles existing between the INS body frame and the camera body frame is required. In addition to this, the offset vector between the onboard GPS and the camera perspective center must also be determined.

The position of the camera perspective centre, as well as the camera orientation at exposure time, are collectively known as the exterior orientation parameters. The interior geometry of the camera sensor, as well as the lens distortion parameters are known as the interior orientation parameters. The exterior orientation parameters are determined using an integrated GPS and INS approach. Interior orientation parameters are determined via laboratory calibration, as has been previously discussed in earlier sections.

“Georeferencing of images can be defined as the problem of transforming the 3-D coordinate vector r^c of the camera frame (c-frame) to the 3-D coordinate vector r^m of the mapping frame (m-frame).” (El-Sheimy, pg 53, 1996). For an integrated sensor system consisting of a camera, GPS and INS, the determination of the coordinates of some object point appearing in the data imagery requires the determination of the coordinate vector which originates from the origin of the mapping frame to the center of the camera system must be determined so that the vector corresponding to the location of the object point in the camera frame can be transferred to the coordinate system corresponding to the mapping frame. Figure 6.1 (which was previously provided, from El-Sheimy, pg 57, 1996) details the relationship between the integrated GPS/INS system and the camera/sensor for a mobile mapping system. This figure is reproduced below for reference:

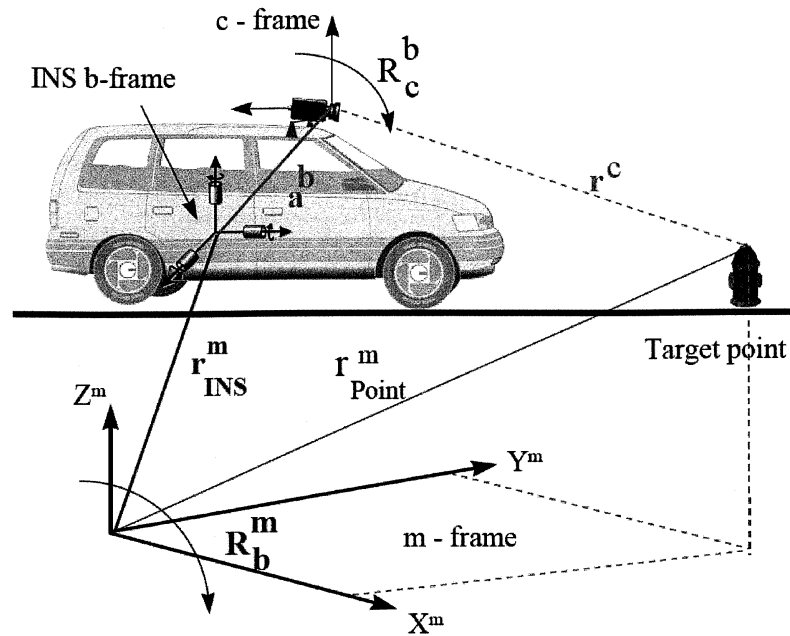


Fig 6.1 - Detailed diagram of elements of georeferencing for the close-range case (El-Sheimy, pg 57, 1996).

In Figure 6.1, the position of the GPS and INS have been consolidated into a single “unit.” As the vehicle is in motion, the location and orientation of the camera frame (c-frame) changes with respect to the mapping frame (m-frame). The georeferencing equation, as given by El-Sheimy (1996) is given below:

$$r_{point}^m = r_{pc}^m(t) + s^i \bullet R_c^m(t) \bullet r^c \quad (6.1)$$

Where:

- r_{point}^m is the coordinate vector corresponding to the location of the target point in the mapping frame,
- $r_{pc}^m(t)$ is the coordinate vector corresponding to the location of the camera perspective centre in the mapping frame,
- s^i is a scale factor which is “specific to a one-point/one-camera combination which relates the image coordinates to the object coordinates.” (El-Sheimy, pg 54, 1996),
- $R_c^m(t)$ is the rotation matrix which rotates the camera frame into the mapping frame,

- r^c is the coordinate vector corresponding to the location of the target point in the camera frame.

However, there is one significant problem associated with Equation 6.1. The problem occurs with the vector $r_{pc}^m(t)$. The equation assumes that the 3-D location of the camera perspective centre can be directly measured. However, this is not the case. Instead, modifications to the equation must be made to reflect the indirect determination of the vector $r_{pc}^m(t)$. This is done by determining the 3D location of the INS body frame, and then determining the relatively small translations and rotations which exist between the INS body frame and the camera frame.

The vector which corresponds to the location of the INS body frame in the mapping frame can be denoted as $r_{INS}^m(t)$, the rotation matrix which rotates the body frame into the mapping frame can be denoted as $R_b^m(t)$ and the constant vector between the camera frame and the INS body frame can be denoted as a^b . With these new parameters, the coordinate vector corresponding to the location of the camera perspective centre in the mapping frame can be re-written as follows:

$$r_{pc}^m(t) = r_{INS}^m(t) + R_b^m(t) \bullet a^b \quad (6.2)$$

Aside from these parameters, the rotation between the camera frame and the body frame must also be determined. In Figure 6.1, this is denoted by R_c^b , is considered a constant and is determined by calibration. With this new rotation matrix, the rotation between the camera frame and the mapping frame $R_c^m(t)$ can be re-written as follows:

$$R_c^m(t) = R_b^m(t) \bullet R_c^b \quad (6.3)$$

If the Equations 6.2 and 6.3 are substituted into Equation 6.1, then the following equation results for the determination of the vector coordinates of a point in the mapping frame. (From El-Sheimy, pg 58, 1996).

$$r_{point}^m = r_{INS/GPS}^m + R_b^m(t)[s^i R_c^b r^c + a^b] \quad (6.4)$$

This equation implies that the coordinate vector of an object point in the mapping frame can be determined by the real-time measurement of the vector $r_{INS/GPS}^m$ and rotation matrix $R_b^m(t)$, as well as two sets of parameters determined via calibration (R_c^b and a^b) and a quantity which can be determined in post mission (r^c). The scale factor s^i changes with distance from

the camera to the object of interest, and is determined via measurement. The parameters R_c^b and a^b are known as bore-sight angles and lever arms, respectively. Methods to determine these quantities will be discussed herein.

6.1 Bore-sight Angle Determination

As mentioned in the previous section, the bore-sight angles are the small rotational offsets existing between the INS body frame and the camera body frame, denoted in Figure 6.1 as R_c^b . Two methods of determining the bore-sight angles will be discussed.

Method 1

In order to determine the bore-sight angles, a calibration which includes the presence of Ground Control Points is required. These can be acquired for a particular area which will be chosen for the calibration, using surveying techniques and/or GPS methods. Care should be taken to ensure that accurate GCPs are collected in the calibration area. Once the GCPs have been established, they must be imaged using the mobile mapping platform. This can be done by driving the mobile mapping platform through the calibration area, and capturing images of the surrounding calibration field using the dodecahedron camera. Observed image points for each GCP appearing in the images are then acquired directly from the images.

The bore-sight angles are then, “calculated by iterative least squares adjustments of the linearised collinearity equation of the GCPs.” (Holzwarth et al., 2005). The mapping equation which maps the 2D image space points to the 3D mapping space points is given below, from Zagajewski, et al.(2005), and modified to reflect the parameters in Figure 6.1:

$$r_{point}^m = r_{pc}^m(t) + s^i R_b^m(t) R_c^b r^c \quad (6.5)$$

Where:

- r_{point}^m is the location of the GCP in the mapping frame (known quantity, from calibration survey)
- $r_{pc}^m(t)$ is the location of the perspective center of the camera in question (known quantity, determined from bundle adjustment)
- s^i is the scale factor as previously defined

- $R_b^m(t)$ is the rotational offsets between the body frame and the mapping frame (known quantity, measured by Inertial Measurement Unit component of INS)
- R_c^b is the bore-sight angles which are required (unknown)
- r^c is the vector of the object point in question, given in the camera frame.

The observation equation is linearised for each GCP observation for each camera with respect to the unknown quantities (R_c^b) to be estimated. A least-squares adjustment is performed and the result gives the bore-sight angles for each camera in the dodecahedron array.

Method 2

An alternative approach to the method given above to obtain the bore-sight angles between each camera in the spherical camera body and the INS body frame can be obtained by following Method 1 for one of the cameras (for simplicity sake, choose the top camera). Since the relative orientation parameters existing between each camera in the dodecahedron array are already determined, only the bore-sight angles between the INS body frame and the camera on the top face of the dodecahedron must be determined, and then those bore-sight angles are adjusted according to the relative orientation information previously obtained. Although this method is less intensive, it may not be as accurate as Method 1, and would be dependant on how accurately the relative orientation parameters related to the dodecahedron array were determined.

6.2 Lever Arm Determination

After a calibration has been performed and a bundle adjustment has been performed to obtain the exterior orientation parameters of each camera, the offset vector between the INS body frame and the cameras can be determined. From El-Sheimy (1996), the equations required to retrieve the offset vectors are given below:

$$a_{ci}^b = R_m^b \cdot \begin{vmatrix} X_{INS}^m - X_{ci}^m \\ Y_{INS}^m - Y_{ci}^m \\ Z_{INS}^m - Z_{ci}^m \end{vmatrix} \quad (6.6)$$

$$a_{GPS}^b = R_m^b \cdot \begin{vmatrix} X_{INS}^m - X_{GPS}^m \\ Y_{INS}^m - Y_{GPS}^m \\ Z_{INS}^m - Z_{GPS}^m \end{vmatrix} \quad (6.7)$$

Where:

- a_{ci}^b is the offset vector between each camera and the INS, expressed in the INS body frame,
- a_{GPS}^b is the offset vector between the INS and GPS, expressed in the INS body frame,
- R_m^b is the rotation matrix which rotates from the mapping frame to the body frame,
- $X_{INS}^m, Y_{INS}^m, Z_{INS}^m$ are the coordinates of the INS in the mapping frame,
- $X_{ci}^m, Y_{ci}^m, Z_{ci}^m$ are the coordinates of the camera perspective center in the mapping frame,
- $X_{GPS}^m, Y_{GPS}^m, Z_{GPS}^m$ are the coordinates of the GPS in the mapping frame.

Again, this can be done to determine the offset vectors between the INS and each camera in the spherical camera configuration. Similarly to the section on bore-sight angle determination, one could alternatively determine the offset vectors between the body frame and a single camera, and then propagate this offset vector according to the relative orientation parameters inherent to the dodecahedron body.

7. Image Mosaicking with a Spherical Camera

Often times during the course of a photogrammetric survey, it is not possible to completely image an area under investigation with a single image. Examples of this include agricultural surveys and geological surveys (in the aerial photogrammetric case), where the region being surveyed is so large that the field of view of the image acquisition sensor is not adequate enough to capture the entire area in a single image. In cases such as these, it often becomes necessary to acquire multiple images of the survey region, and then fuse these images together to form one large image. This large image is the equivalent image which would be obtained by an imaging sensor with a much larger field of view. This image fusing process is known as image mosaicking, and is crucial if one intends to compose a completely immersive image using a spherical camera. From Hall (1996), a typical image mosaicking application should contain the following:

- Geometric corrections
- Gray level corrections and seam elimination.

Geometric corrections are essentially a series of corrections or processes by which an image point is mapped to a new location (Hall, 1996). In the case of the spherical camera, one must view the world as a “spherical” world, where each point in the real world, appearing in the image, must be thought of as residing on the surface of a “sphere” in the real world, centered at the centre of the dodecahedron. This is because in close-range photogrammetry cases, it is often very difficult to obtain “depth” information (i.e., how far away an object is from the camera). In the aerial photography case, depth information is readily available; however this is much more difficult to obtain in close-range photogrammetric surveys. A proposed method for mosaicking imagery captured by the spherical camera will be discussed in this section.

Aside from the mosaicking/geometric correction aspect, portions of the images which overlap with each other must be dealt with. Finally, a colour-balancing and seam line elimination method must be employed. This is often required due to the fact that each camera’s radiometric specifications may differ from one another’s. Thus, if colour-balancing and seam line elimination is not performed, the image mosaic may appear “patchy”, and each scene of the mosaic may be easily delineated from one another. This is an undesirable effect of image mosaicking, and must be dealt with. Possible methods for colour-balancing imagery captured by the spherical camera will also be dealt with in this section.

7.1 Geometric Correction for Image Mosaicking

In order to mosaic imagery captured by the spherical camera to produce a 360 degree panoramic image, the images are projected onto the surface of a sphere. In order to do this, the assumption that each camera in the dodecahedron array is centered at the same point (i.e., at the center of the dodecahedron) is made. In reality, this is not the case; however this assumption can be made given the knowledge that in reality, the perspective centers of the cameras in the dodecahedron array are offset from each other by only a few centimeters. If a sphere is chosen to project our images onto in such a way so that the radius of this sphere is large enough to compensate for the error in making the assumption that each camera is centered at the same point, then this error can be considered negligible.

The process for projecting an image onto the surface of a sphere is given below for one of the cameras. The same process can be repeated for each image of the scene from each camera to form the panoramic strip.

1) For each pixel which comprises the image in question, the positions of the points located on the surface of the sphere are computed. This is illustrated in Figure 7.1, where the camera is centered at the center of the dodecahedron (which is also centered at the center of the sphere), and the corner coordinates of the image are projected onto the sphere.

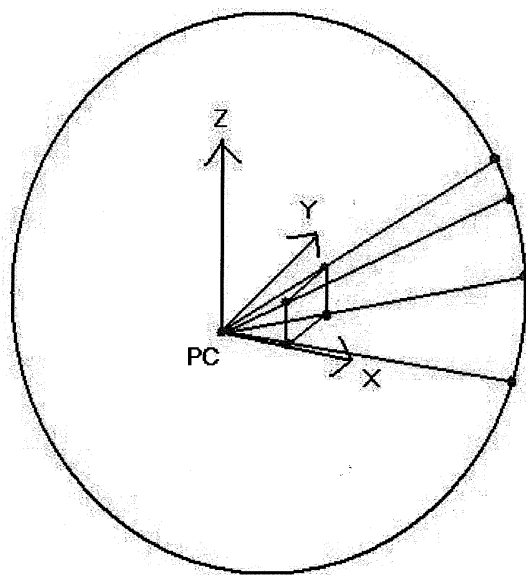


Fig 7.1 – Projecting image onto surface of the sphere

The equation used to compute the coordinates of the edge points on the surface of the sphere is given below:

$$\begin{bmatrix} X \\ Y \\ Z \end{bmatrix}_{SPH} = \begin{bmatrix} X \\ Y \\ Z \end{bmatrix}_{PC} + r \cdot M_{ROT} \cdot \begin{bmatrix} x \\ y \\ -f \end{bmatrix}_{img} \cdot \frac{1}{\sqrt{x^2 + y^2 + f^2}} \quad (7.1)$$

Where:

- X,Y,Z are the Cartesian coordinates of the image point projected onto the sphere
- r is the radius of the sphere being projected onto
- M_{ROT} is the rotation matrix
- x, y are the image coordinates in the image coordinate system
- f is the focal length of the camera

2) Once the coordinates of the edges of the image have been projected onto the sphere, they are converted into spherical coordinates (ϑ, λ, r) as follows:

$$r = \sqrt{X^2 + Y^2 + Z^2} \quad (7.2)$$

$$\vartheta = \tan^{-1}\left(\frac{Y}{X}\right) \quad (7.3)$$

$$\lambda = \cos^{-1}\left(\frac{Z}{R}\right) \quad (7.4)$$

3) Since the coordinates of the edges of the image, projected onto the sphere, are now available in spherical coordinates, the information provided in Figure 7.2 can be used (provided by Immersive Media). Figure 7.2 depicts a mosaic generated using data from the Dodeca 2360. Figure 7.3 depicts a spherical coordinate system superimposed over the mosaic. Angles (ϑ) are along the X axis and range from -180 degrees to + 180 degrees. Angles (λ) are along the Y axis and range from -90 degrees to + 90 degrees.



Fig 7.2 – Mosaic generated by Immersive Media using data captured by Dodeca 2360

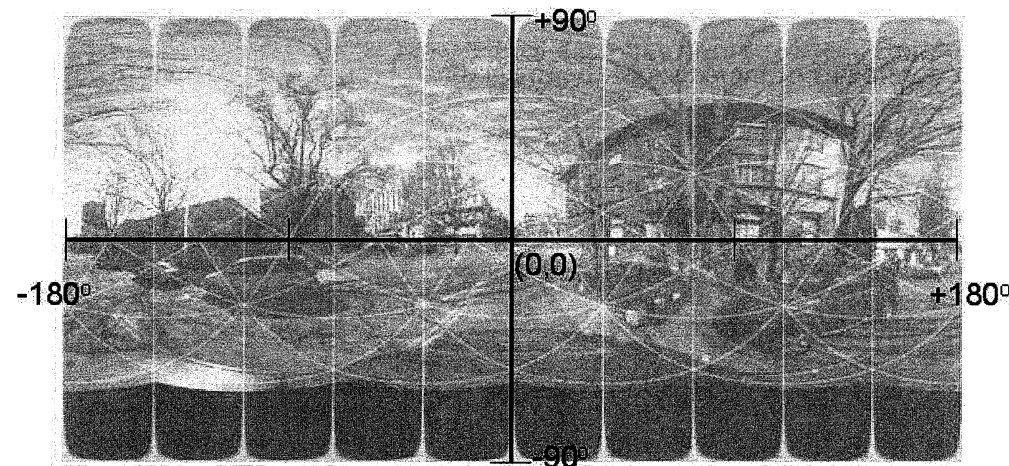


Fig 7.3 – Super-imposed spherical coordinate system on mosaic

On Figure 7.3, the edge points of an image can be plotted (projected onto the sphere in spherical coordinates). This is shown in Figure 7.4:

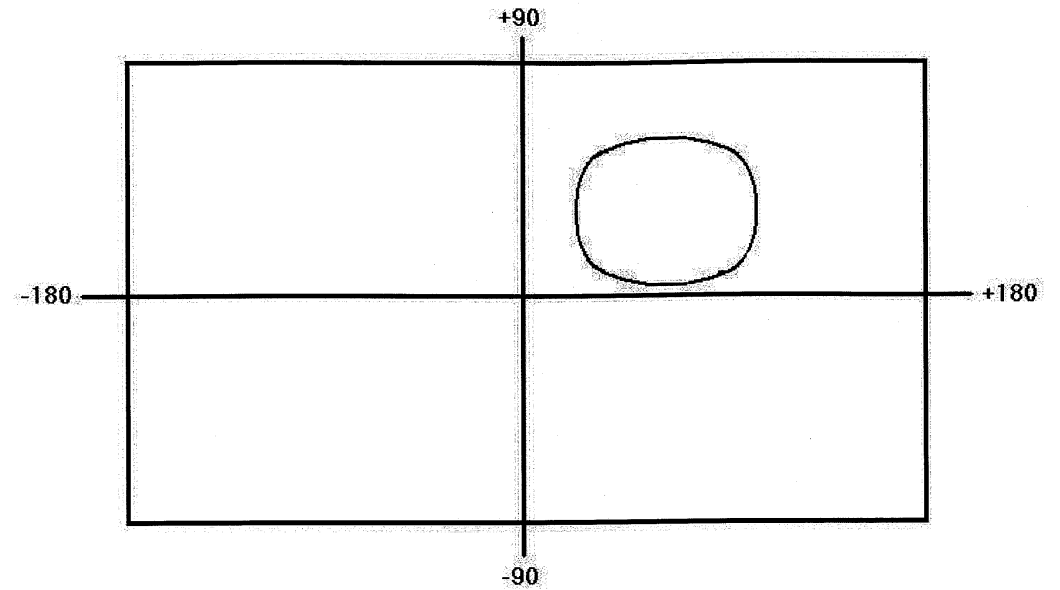


Fig 7.4 – Image edge points plotted onto Immersive Media mosaic grid

A minimum bounding box which completely encompasses the image plotted onto the immersive media mosaic grid is formed. This is shown in Figure 7.5:

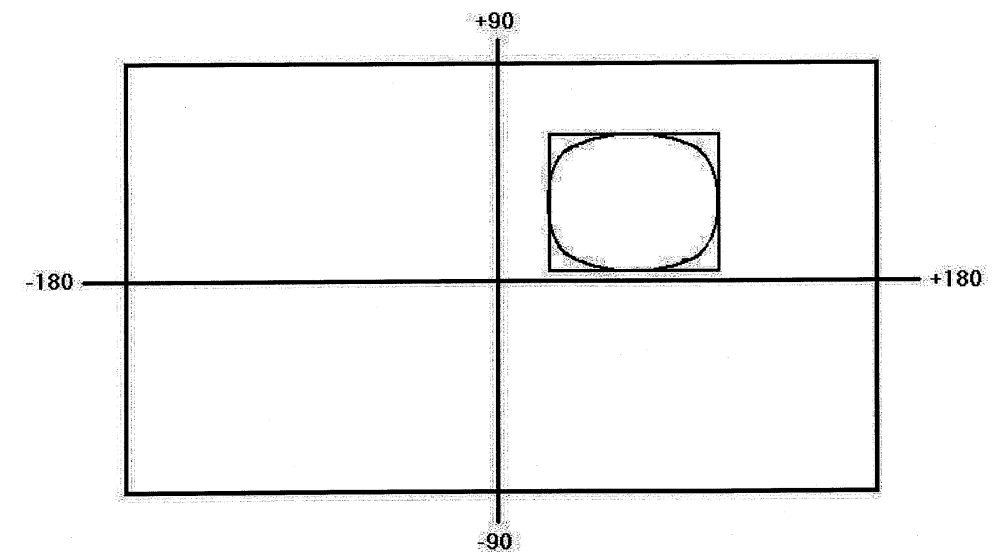


Fig 7.5 – Minimum Bounding box encompassing image on mosaic

4) For each pixel in the minimum bounding box, the corresponding spherical coordinates from the Immersive Media image are converted back to Cartesian coordinates X,Y,Z according to the following:

$$X = r \cos \vartheta \sin \lambda \quad (7.5)$$

$$Y = r \sin \vartheta \sin \lambda \quad (7.6)$$

$$Z = r \cos \lambda \quad (7.7)$$

These points are then converted to image x, y using the collinearity equations and the exterior orientation and interior orientation defined for the camera whose image is under investigation. A test is then performed to check if the image x, y computed falls within the image under investigation. If it does, it is included in the mosaic in its respective position otherwise it is omitted.

This procedure can then be repeated for each image captured by the Dodeca 2360, to form the mosaic. One can then proceed to color balancing and seam line elimination techniques to improve the visual quality of the mosaiced image. This will be discussed in the next section

7.2 Color Balancing and Seam Line Elimination

When mosaicking imagery, it is often the case that imagery acquired may have been acquired under different conditions (i.e., different day, time, season, year, etc). In the case of a spherical camera, it may also be the case that one camera may view something that has a shadow, but from another camera's point of view that shadow is not present. When this occurs, the radiometric properties of a scene may differ from one image to another. This is dependent on when the imagery was acquired relative to the other imagery in the full "data set", as well as the various cameras which were used to acquire the data. When these radiometric differences are not accounted for, the resulting mosaic is not "visually appealing" in that one can clearly perceive seam lines. The over-all effect is that of a "patch-work" looking mosaic, where each image in the mosaic can be clearly delineated from another. In some cases, the effect is not very noticeable. As Guindon, 1997 notes, "images of agricultural areas are comparatively simple to visually integrate primarily because such scenes are 'busy', i.e. they contain a patchwork of small areas of diverse reflectance, thereby making it difficult to visually follow an inter-scene boundary." At the same time however, Guindon, 1997 makes mention of the fact that a mosaic of an agricultural area, especially when the images composing the mosaic are acquired during different growing seasons, contain very little information continuity across the entire scene. Therefore, in order to obtain a visually appealing mosaic, one must perform some colour-balancing / radiometric correction / seam line elimination techniques. This section will discuss a

possible method to colour-balance a mosaic generated from a spherical camera. It will also discuss the seam line elimination, as well as seam line smoothing.

7.2.1 Colour Balancing (Histogram Matching)

As made note of in the previous section, often times when creating a mosaic from various sets of imagery, the result is a patch-work like appearing mosaic, and "the creation of spurious artificial 'edges' at the seams between the pictures sections (tiles). These artificial edges occur when there are perceptible differences between the tiles within the region of overlap." (Milgram, 1975). In order to obtain a visually appealing mosaic, these visual differences between imagery must be dealt with. In the case where imagery has been obtained via airborne or satellite methods, colour balancing can become even more bothersome due to atmospheric effects, clouds, snow, water, etc. all of which cause grey level differences between imagery in the mosaic. In the close range photogrammetry case (such as our spherical camera configuration), these effects are not an issue since the system is not imaging through the atmosphere. However, there will be numerous sharp terrain changes occurring all around the spherical camera, and as such colour balancing is still necessary.

For decades, researchers have worked extensively to develop good colour balancing techniques. Among the various colour balancing methods in existence, one of the most commonly utilized methods employed today is based on histogram matching techniques. Milgram, 1975, provides a method which takes advantage of histogram matching to obtain a colour balanced mosaic. This method will be described herein, as the approach taken can be applied to a spherical camera setup.

The first step in Milgram's colour balancing approach is to locate the overlap region for the imagery under investigation. Once the overlap region has been identified between two or more images, a grey-level histogram for the overlap region for each image is obtained. As Milgram notes, one would ideally hope that the histograms in the overlap region for each image would match. However, this is normally not the case due to differences in the imaging sensor, as well as atmospheric effects, etc. To compensate for these differences, a zeroth order, or first order adjustment method is employed that essentially shifts the histograms in such a way as to make their averages coincide. Although this method may help to balance the colour, tonal and contrast visual appearance of the imagery, it is still not perfect as the edges of the imagery will

still be visible. As such, Milgram notes, this step should be used as a pre-processing step to the seam definition and smoothing step.

7.2.2 Seam Line Definition

The seam line definition process, as outlined by Milgram, is meant to, “choose points in the overlap region which define where one tile ends and the other tile(s) begins.” (Milgram, 1975). One method of doing this is to scan the overlap region, one “row” at a time, and choose one point per line in the overlap region. In Milgram’s algorithm, image information from to the left of the point in question comes from the line segment of the left hand tile, whereas the information that comes to the right of the point will come from the right hand tile. From Milgram, 1975, the seam point for a single line is chosen as follows:

- Let L_1, \dots, L_k be the grey level values of the current line in the left hand images’ overlap region
- Similarly, let R_1, \dots, R_k be the grey level values of the current line in the right hand images’ overlap region.
- K = width of overlap region, in pixels
- A seam point for each line is then chosen in such a way as to minimize the presence of an artificial edge. The edge measure, as given by Milgram, is reproduced below, where the sums of the differences are computed over w points. The goal is to identify the index j where D_j is minimal. j ranges from $w/2$ to $K - w/2$:

$$D_j \equiv \sum_{i=-w/2+1}^{w/2} |L_{j+i} - R_{j+i}| \quad (7.8)$$

This seam point definition scheme results, “[in] a succession of points whose horizontal positions are unrelated to one another.” (Milgram, 1975). The random positioning of the edge, “is known as ‘feathering’, and help[s] to reduce the visual cues which would normally attract the eye to the seam.”

7.2.3 Seam Smoothing

After the seam points have been identified as outlined in Section 7.2.2, a smoothing process is required so that any sudden changes in grey level values surrounding the seam point are diminished. The procedure given below, as outlined by Milgram, 1975, provides a final

mosaic image in which colour, tonal and contrast balancing has been achieved, and where seam lines are effectively hidden:

- For seam point s , let D_s = the minimum edge difference at seam point s
- $H = \frac{D_s}{w}$ is then the average difference in grey level corresponding to overlap mismatch existing between left and right sides of composite line.
- “Smoothing at s involves apportioning H among the neighbours of s to the right and left so that there is a gradual transition or ramp effect.” (Milgram, 1975)

The slope of the ramp indicates how many of the neighbouring points are affected by the smoothing process. If one wishes to hide the seam line in the best possible way, a “ramp” with a more gradual slope can be applied. However, the trade-off here is that the information around the seam point is “tainted” as the contrast level of these neighbouring points are altered.

This method offers a suitable approach for hiding the seam line(s) in a mosaic. For a spherical camera setup, the same approach could be applied, and performed on a “sequential” basis. This means that in the event that three images, for example, overlap the same area, then one can perform the seam line identification and feathering methods for two of these images, and then use the results to identify the seam line between the results from the previous two images, and the third image, and finally feathering. Such an approach can be repeated for all overlapping areas in the imagery.

7.3 Potential Problems with Approach

Although the methods of mosaicking and colour balancing presented in this section appear to be sufficient, there are several shortcomings which need to be addressed. The first issue that arises occurs when the cameras of the dodecahedron array view an object in the scene from different angles whereby the amount of sunlight incident on the surface of the object and recorded by the sensor varies with respect to the angle at which it is received by the sensor. In such instances, it may be possible that the same object appears to be a different object in a set of overlapping images. If the histogram colour balancing technique described in the preceding section is applied, the differences in grey level between the two images in the overlapping regions may differ significantly enough that the correction applied to one of the overlapping images may overcompensate for the effect.

Other issues which may crop up occur when an object appears in the overlap area of one image, but not the other. Such instances may occur when one camera captures the presence of a person walking on the street, and that same person may not appear in one of the other images. When comparing the grey level differences between the two images in the overlapping region, the problem becomes more apparent. In such cases, a special modification to the colour balancing technique described previously will need to be employed so as to remove varying grey level pixels between the two images in the overlap region. Such algorithms which may be employed could be those used routinely in satellite and airphoto mosaics, where clouds may be present in one image and not the other. An example of this technique can be viewed in Scholten, 1996, where Scholten explains a method to eliminate spurious pixels and obtain proper grey level values for pixels in overlap areas using a weighting function. Guindon, 1997, also outlines a method to deal with colour balancing in similar areas using grey level scattergrams.

A final issue which could arise occurs when considering the mis-registration between two overlapping images in the scene. In the previous sections, the assumption was made that all of the cameras in the dodecahedron array could be considered to be centered at the same point. However, this is not the case, and as such this discrepancy will result in a mis-registration between the two images, making colour balancing and seam line elimination more difficult. One potential solution to this problem could be to down sample the images just enough so as to compensate for the mis-registration error. An example of this would be to take 4 pixels in the affected area, and make it one pixel in a "new" down-sampled image. Care would have to be taken to ensure that the down-sampling process would not destroy the desired accuracy and spatial resolution in the final product.

8. Conclusions and Future Work to be Done

This research paper focused on various methods and approaches one would need to explore when considering the use of a spherical camera in mobile mapping applications, as opposed to the standard "multiple camera" approach. Such an approach would be very beneficial for transportation departments, who routinely operate mobile data acquisition systems which rely on a series of cameras mounted on the vehicle. This type of system would be beneficial in providing the respective departments with complete data coverage, something for which traditional methods fail to realize. The standard approach (multiple cameras) serves to provide only part of the picture. Surveying techniques provide only point information, rather than continuous coverage. Only through the use of a spherical camera can the "complete picture" be efficiently formed. The combination of this system with existing sensors in use by transportation departments creates a truly robust and complete data acquisition system.

This paper demonstrated methods of developing a "math model" for a spherical camera such as the Dodeca 2360 by considering the geometric shape for which it is based on. Results of this method were tested against various plotting software, and further confirmed through the use of a self-calibrating bundle adjustment. The bundle adjustment software developed not only served this purpose, but also provided a means of determining interior and exterior orientation information for such a camera system.

Future work required as outlined in this project includes the computer implementation of the mosaicking and colour balancing techniques for use with the spherical camera proposed. The ground work has essentially been laid for a software developer to program the mosaicking and colour balancing techniques, in combination with the self-calibrating bundle adjustment program developed already, and the bore-sight and lever arm determination algorithms, to complete the software package. In addition, further refinements to the mosaicking method to compensate for the assumption made of all cameras being located at the same point should be explored, as well as other methods to eliminate spurious grey level pixels attributed to sudden changes in overlapping imagery should also be undertaken.

9. References

- Cramer, M. and Stallmann, D. (2001)**, "On the use of GPS/Inertial Exterior Orientation Parameters in Airborne Photogrammetry", The Institute for Photogrammetry, University of Stuttgart.
- Ebadi, H. (1997)**, "GPS Assisted Aerial Triangulation", PhD Thesis, Department of Geomatics Engineering, University of Calgary, Canada.
- El-Sheimy, N. (1996)**, "The Development of VISAT – A Mobile Survey System for GIS Applications", PhD Thesis, Department of Geomatics Engineering, University of Calgary, Canada.
- Guindon, B. (1997)**, "Assessing the Radiometric Fidelity of High Resolution Satellite Image Mosaics", ISPRS Journal of Photogrammetry and Remote Sensing, 1997, Vol 52, pages 229 – 243
- Guindon, B., et al, (2003)**, "From Need to Product: A Methodology for Completing a Land Cover Map of Canada with Landsat Data", Canada Centre for Remote Sensing, Canadian Forest Service, University of Lethbridge, Pacific Forestry Centre. Preprint edition.
- Hall, R.W. and Gumustekin, S. (1996)**, "Mosaic Image Generation on a Flattened Gaussian Sphere", Proceedings 3rd IEEE Workshop on Applications of Computer Vision, Dec 2-4, 1996. Pages 50-55
- Holzwarth, S., Muller, R. and Simon, C. (2005)**, "Determination and Monitoring of Boresight Misalignment Angles During the HYMAP Campaigns HYEUROPE 2003 and HYEUROPE 2004", Proceedings of 4th EARSel Workshop on Imaging Spectroscopy, pages 91 – 100.

- Milgram, D.L. (1975)**, "Computer Methods for Creating Photomosaics", IEEE Transactions on Computers, Nov. 1975, Volume C-24, Issue 11, Pages 1113-1119
- Scholten, F. (1996)**, "Automated Generation of Coloured Orthoimages and Image Mosaics Using HRSC and WAOSS Image Data of the MARS96 Mission", International Archives of Photogrammetry and Remote Sensing. 1996. Vol. XXXI, Part B2, pages 351 – 356
- Schwarz, P. and El-Sheimy, N. (2004)** "Mobile Mapping Systems – State of the Art and Future Trends", Department of Geomatics Engineering, University of Calgary, Canada.
- Wiedemann, A. More, J. and Tauch, R. (2003)**, "Archimedes3D – An Integrated System for the Generation of Architectural Orthoimages" FPK Ingenieur GmbH, Feurigstr 54, 10827 Berlin, Germany.
- Wolf, P. and Dewitt, B. (2000)**, "Elements of Photogrammetry with Applications in GIS", 3rd edition, USA: McGraw-Hill, ISBN 0-07-292454-3